Excitation of airwaves caused by bubble bursting in a cylindrical conduit: Experiments and a model

Tsukasa Kobayashi,[1] Atsuko Namiki,[2] and Ikuro Sumita[1]

Received 29 July 2009; revised 13 June 2010; accepted 30 June 2010; published 6 October 2010.

[1] Strombolian eruptions are considered to be a consequence of the bursting of a large bubble. In order to understand the relation between the style of bubble bursting and the resulting airwave, we perform experiments of bubble bursting at the top of the surface of viscous liquid contained in an acrylic pipe which acts as an air column and observe it visually and acoustically. We find that when the liquid viscosity is less than 1 Pa s, the bubble vibrates before bursting. The major source of the airwave during the sequence of the bubble bursting is the bubble vibration. On the other hand, when the liquid viscosity is greater than 1 Pa s, the bubble does not vibrate. During bubble bursting, an aperture appears on the bubble film. The aperture growth first accelerates and later decelerates before finally stopping. The major source of the airwave is the aperture growth. We calculate a synthetic waveform of the airwave generated by the aperture growth which explains the experimentally observed airwave well. When the frequency of the airwave generated by the aperture growth matches the eigenfrequency of the air column, resonance occurs. Applying this model to the Strombolian eruption, the characteristic low frequency (<20 Hz) is explained if the velocity of the aperture growth is several meters per second. The model also explains the asymmetrical initial rise of the airwave observed in the Strombolian eruptions as a result of the accelerating growth of the aperture.

Citation: Kobayashi, T., A. Namiki, and I. Sumita (2010), Excitation of airwaves caused by bubble bursting in a cylindrical conduit: Experiments and a model, *J. Geophys. Res.*, *115*, B10201, doi:10.1029/2009JB006828.

1. Introduction

[2] Strombolian eruptions have been considered to be a consequence of the bursting of a large bubble [e.g., *Blackburn et al.*, 1976; *Wilson*, 1980; *Jaupart and Vergniolle*, 1988; *Parfitt*, 2004; *Harris and Ripepe*, 2007; *Houghton and Gonnermann*, 2008]. This large bubble forms from the coalescence of small bubbles [e.g., *Jaupart and Vergniolle*, 1988; *Ripepe and Gordeev*, 1999; *James et al.*, 2004] at deeper parts of the conduit [*Burton et al.*, 2007; *Edmonds*, 2008]. In order to understand the characteristics of the large bubble, observation of the airwaves associated with the eruption is an effective method [e.g., *Vergniolle and Brandeis*, 1994; *Ripepe and Gordeev*, 1999]. This is because diffraction and scattering of airwaves in the atmosphere is small [*Garces et al.*, 1999; *Johnson et al.*, 2004]. An important feature of the airwave is its very low frequency (<20 Hz) such that it is recognized as an infrasonic or infrasound wave [e.g., *Vergniolle and Brandeis*, 1994; *Ripepe et al.*, 1996; *Hagerty et al.*, 2000; *Rowe et al.*, 2000; *Caplan-Auerbach and McNutt*, 2003; *Johnson et al.*, 2004]. We here use "airwave" for an airborne acoustic wave as a generic term for sound, infrasound, and infrasonic waves. The source of the airwaves observed during a Strombolian eruption is explained mainly by a monopole with a minor contribution from dipole radiation [*Johnson et al.*, 2008].

[3] Explosive release of a pressurized gas generates an airwave [e.g., *Johnson et al.*, 2004]. This process can sometimes be visually observed [*Yokoo and Taniguchi*, 2004] and has been simulated by experiments and numerical calculations [*Kieffer and Sturtevant*, 1984; *Morrissey and Chouet*, 1997]. When bubbles burst without magmatic eruption, airwaves which sometime correlate with tremors are generated [*Ripepe et al.*, 1996; *Lees et al.*, 2004]. This process may be analogous to the bursting of a balloon, which is considered as instantaneous removal of the membrane [e.g., *Deihl and Carlson*, 1968]. The estimated frequency by instantaneous removal of the bubble film (>100 Hz) is higher than the observed low frequency of the airwave during the Strombolian eruption (<20 Hz) [*Vergniolle and Brandeis*, 1994].

[4] We know from experience that when we prick a balloon with a needle, a loud sound is generated. This is because when the balloon film ruptures, it immediately shrinks due to its elasticity before the pressurized gas contained within the balloon can expand. As a result, pressure discontinuity with the shape of the burst balloon forms. The pressure discontinuity travels and we hear it as a loud sound. However, if the aperture made by a needle does not grow, the balloon may not explode so that we do not

[1] Graduate School of Natural Science and Technology, Kanazawa University, Kanazawa, Japan.
[2] Department of Earth and Planetary Science, University of Tokyo, Tokyo, Japan.

0148-0227/10/2009JB006828

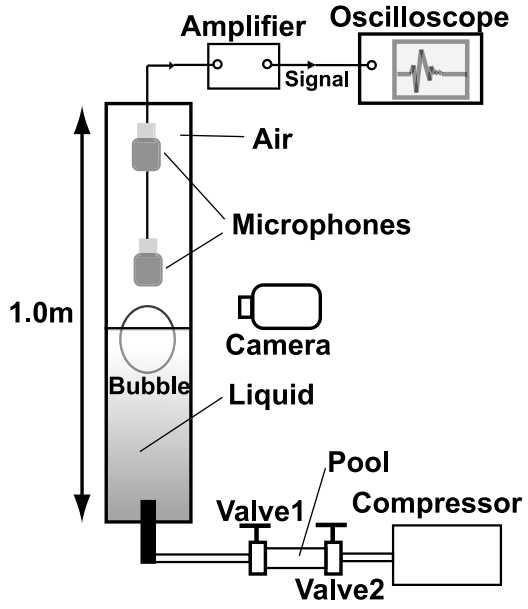

Figure 1. Schematic diagram of the experimental apparatus.

hear a loud sound; instead, the air may escape through the aperture as it makes a hissing sound. This thought experiment suggests that the waveform of an airwave generated by a bubble bursting during a Strombolian eruption depends on how the bubble film opens. Indeed, when a balloon film is removed under a finite velocity, the observed waveform differs from the ideal N wave [*Kulkarny*, 1978]. In addition, the importance of the timescale of the film removal for the acoustic emission by bubble bursting has been recognized [*Vidal et al.*, 2006; *Divoux et al.*, 2008].

[5] It has been recognized that an aperture which has formed on a soap film grows at a constant velocity [*Taylor*, 1959; *Culick*, 1960]. On the other hand, recent experimental studies have revealed that when the viscosity of the bubble film is sufficiently large, the aperture growth velocity is time dependent; it first accelerates and then decelerates [*Debregeas et al.*, 1995, 1998]. The aperture growth finally stops and the bubble film deflates under its own weight [*da Silveira et al.*, 2000]. The airwave excited by these types of bubble bursting may have a different frequency from the N wave excited by the instantaneous film removal.

[6] Another possible mechanism of the airwave during a Strombolian eruption is resonance. It is widely recognized that a bubble resonates and generates sounds [e.g., *Leighton*, 1994]. *Vergniolle and Brandeis* [1996] suggests that the vibration of a large bubble generates an airwave. A magma-filled conduit may also become a resonator [*Buckingham and Garces*, 1996; *Garces and McNutt*, 1997]. During the bubble bursting, an aperture forms on the bubble film. This geometry can act as a Helmholtz resonator [*Spiel*, 1992; *Vergniolle and Caplan-Auerbach*, 2004; *Cannata et al.*, 2009]. When there is a gas supply, the same geometry gives rise to another pressure oscillation [*Hellweg*, 2000]. After the bursting of a vertically elongated bubble, a vertical cavity remains which may act as an air column resonator [*Divoux et al.*, 2008; *Cannata et al.*, 2009]. Seismological observations have revealed that some resonators are situated around the vent and cause long-period (LP) or very long period (VLP) seismicity before the eruption [e.g., *Neuberg et al.*, 1994; *Rowe et al.*, 2000; *Aster et al.*, 2003; *Chouet*, 2003].

[7] In order to estimate the details of the large bubble, such as the size and overpressure which causes the Strombolian eruption from the airwave, we need to know the relation between the bubble bursting, including the resonance system, and the resulting waveform of the airwave. We experimentally simulate this system by a bubble bursting in a long acrylic pipe. Similar systems have been investigated experimentally [*Seyfried and Freundt*, 2000; *Ripepe et al.*, 2001; *James et al.*, 2004, 2006]. *James et al.* [2004] shows that bubble bursting at the surface causes airwaves when the liquid viscosity is sufficiently low. *Ichihara et al.* [2009] measures the airwave generated by underwater explosion and discusses the relation between the measured airwave and visual observation.

[8] In this study, we first experimentally investigate how the vibration and rupture of a bubble film emit an airwave by using both visual and acoustic measurements with various liquid viscosities. Next, we make a model for the airwave generated by a film rupture and discuss the relation between the waveform and air column resonance. Finally, we apply our model to Strombolian eruptions.

2. Possible Airwave Sources

[9] We perform experiments with the apparatus shown in Figure 1. The acrylic pipe is filled halfway with a liquid; thus the upper and lower parts of the pipe become air and liquid columns, respectively. This system represents a volcanic conduit filled halfway with a magma. A bubble ascends in the liquid and bursts at the surface. This system generates several kinds of airwaves. We here summarize the possible airwave sources.

2.1. Air Column Resonance

[10] The unfilled pipe or a volcanic conduit can become an air column resonator. The resonance frequency for the air column with a length L with one side open and the other one closed is expressed as [e.g., *Yoshikawa and Fujita*, 2002]

$$f_a = \frac{(2n+1)c_a}{4(L+\delta L)} \qquad n = 0, 1, 2, \ldots, \tag{1}$$

where c_a is the air sound velocity and δL is the open-end correction and is approximately 0.6 times the pipe radius a. The effective length of the open tube for acoustical purposes, $L + \delta L$, is longer than the actual length, L [e.g., *Blackstock*, 2000]. Under the fundamental mode, the wavelength is four times the effective column length, where the open end is a pressure node and the closed end is an antinode. When L = 0.55 m, a = 0.028 m, and c_a = 345 m s^{-1}, which are our typical experimental conditions, the frequency of the fundamental mode is 150 Hz.

[11] When both ends are closed, the resonance frequency is written as

$$f_a = \frac{nc_a}{2L} \qquad n = 1, 2, \ldots, \tag{2}$$

where both ends become the pressure antinodes. The wavelength of the fundamental mode is twice the column length.

[12] We regard the boundary conditions of the volcanic conduit and our experimental setup as closed bottom (surface of magma) and an open top. Before the bubble bursts, the liquid bubble film consists the bottom end. After the bubble bursts, the surface of the liquid column becomes the bottom end. The characteristic impedance of our experimental liquid is $Z = \rho_{liq} c_{liq} > 1.5 \times 10^6$ MKS rayls (kg m^{-2} s^{-1}) which is much larger than that of air, 415 MKS rayls, where ρ_{liq} and c_{liq} are the density and sound velocity of liquid, respectively. Such impedance contrast results in a closed bottom end. This situation is similar to a volcanic conduit filled with magma.

2.2. Bubble as a Source of Airwave

[13] A bubble can become several kinds of resonators as it evolves [*Vergniolle and Brandeis*, 1994; *Vergniolle et al.*, 1996]. As the bubble ascends in a liquid column, it vibrates radially [e.g., *Leighton*, 1994]. When the bubble reaches the surface of the liquid column, the bubble film may vibrate as a membrane [*Vergniolle and Brandeis*, 1996]. During bubble bursting, a bubble has an opening and can act as a Helmholtz resonator [*Vergniolle and Caplan-Auerbach*, 2004]. On the other hand, when the bubble film is removed immediately, it may cause an N-shaped wave [e.g., *Deihl and Carlson*, 1968].

[14] The resonance frequency of a bubble in a liquid neglecting the effect of the surface tension is expressed as [e.g., *Leighton*, 1994; *Blackstock*, 2000]

$$f = \frac{1}{2\pi R_b}\sqrt{\frac{3\gamma P_b}{\rho_{liq}}}, \tag{3}$$

where R_b is the bubble radius, P_b is the static pressure inside the bubble, and γ is the ratio of specific heats. For the air under room temperature, $\gamma = 1.4$. For a bubble with a radius 0.025 m under atmospheric pressure, the resonance frequency is 130 Hz. Equation (3) is derived from the balance between the maximum value of the internal energy of the gas inside the bubble, which is the work done in compressing the bubble from the equilibrium volume V_{eq} to the minimum V_{min} and is written as $-\int_{V_{eq}}^{V_{min}} (P_b - P_{beq})\, dV = 6\pi\gamma P_b R_b R_\epsilon^2$, and the kinetic energy of liquid $m_{rad}(2\pi R_\epsilon f)^2/2$, where $m_{rad} = 4\pi R_b^3 \rho_{liq}$ is called the radiation mass of the bubble, which results from compressing the bubble, and R_ϵ is the amplitude of the bubble vibration [e.g., *Leighton*, 1994].

[15] When the bubble is at the surface, only the bubble film vibrates. The radiation mass of the hemispherical bubble film is $2\pi\rho_{liq} R_b^2 h$, and the frequency of the bubble film vibration becomes

$$f \sim \frac{1}{2\pi}\sqrt{\frac{6\gamma P_b}{\rho_{liq} R_b h}}, \tag{4}$$

where h is the bubble film thickness. This is similar to the equation derived by *Vergniolle and Brandeis* [1996]. For a bubble with a radius 0.028 m and a film thickness of 10^{-4} m, the resonance frequency becomes 2400 Hz.

[16] During bubble bursting, an aperture appears on the bubble film. This shape resembles a bottle which has a chamber and a very short neck and allows the bubble to become a Helmholtz resonator [*Spiel*, 1992; *Vergniolle and Caplan-Auerbach*, 2004]. The resonance frequency of the Helmholtz resonator is

$$f = \frac{c_a R}{2}\sqrt{\frac{1}{\pi l' V}}, \tag{5}$$

where R is the aperture radius, V is the volume of the chamber, and l' is the effective length of the neck. The effective length of the neck is in the range of $8R/3\pi \le l' \le 16R/3\pi$. For a bubble with a radius of $R_b = 0.025$ m and an aperture radius of $R = 0.01$ m, the Helmholtz resonance frequency becomes 920–1300 Hz.

[17] If bubble bursting is caused by the immediate removal of the bubble film covering the over-pressurized gas inside the bubble, an N-shaped wave is generated [e.g., *Deihl and Carlson*, 1968; *Vergniolle and Brandeis*, 1994]. The frequency of this wave is expressed as

$$f = \frac{c_a}{2R_b}. \tag{6}$$

For a bubble with radius 0.025 m, the frequency becomes 6900 Hz.

3. Experimental Procedure

[18] We conduct experiments in an acrylic pipe with 1 m length and an internal diameter of 56 mm to simulate the phenomena inside the volcanic conduit (Figure 1). This setup is frequently used to investigate the slug flow in a volcanic conduit [e.g., *Seyfried and Freundt*, 2000]. Liquid syrup, our analogue magma, is contained in the lower part with a height range of 0.31–0.74 m of the pipe. The bottom of the pipe connects to a gas pool with a given volume (10–72 $\times$ 10^{-6} m^3) and pressure (0.2–0.78 MPa) controlled by a compressor. We checked the volume of the pool by releasing the gas into the water and collecting them with a measuring cylinder.

[19] An air bubble is produced when the gas inside the pool is released into the liquid column. The bubble ascends in the liquid column and reaches the surface. The bubble then bursts and causes pressure fluctuation within the air column. The pressure fluctuation is measured by microphones (Primo EM156S5A) with a sensitivity of 9–12 mV Pa^{-1}, which have a flat response in the frequency band of 1–2000 Hz and a detection range of up to 10^4 Hz. The measured pressure fluctuation is amplified by commercial operational amplifiers and recorded by an oscilloscope (Agilent 54624A) with a sampling rate of 0.5 MHz. The measured waveform is analyzed after reducing the time resolution to 4 $\times$ 10^{-5} s by averaging 20 data. The spectrogram of the pressure fluctuation is obtained by short-time Fourier transform calculated by using Matlab. The sequence during bubble bursting is recorded with a high-speed camera (Ditect HAS-500) that takes 1000 frames per second (fps) with a resolution of 640 $\times$ 480 pixels and a shutter speed 1/5000 or 1/10000. The possible time difference between the visual and pressure measurements is $\le$1 ms. After bubble bursting, we insert a scale inside the air column and calibrate the length scale of the obtained pictures.

[20] For our magma analogue, we use syrup solutions. Syrup is frequently used as a magma analogue because it is a Newtonian fluid and has similar viscosity and surface

Table 1. Experimental Conditions[a]

η_{liq} (Pa s)	V (mL)	L (m)	Freq (Hz)	Lower (Hz)	std(L)	Upper (Hz)	std(U)	Number 1	cL	cU	Number 2
10^{-3}	32	0.55	150	230	150	230	150	4	0.21	0.20	1
10^{-3}	44	0.55	150	150	0	210	140	5	0.29	0.50	3
10^{-3}	52	0.55	150	150	2	300	300	4			0
10^{-3}	56	0.55	150	150	4	150	4	3	−0.71	−0.71	1
10^{-3}	57	0.55	150	150	2	150	2	2			0
10^{-3}	58	0.55	150	150	0	150	0	1			0
10^{-3}	77	0.55	150	150	3	190	110	7	0.57	0.33	2
0.17	8	0.62	140	680	0	680	0	1			0
0.17	32	0.62	140	680	2	680	2	2			0
0.17	56	0.62	140	680	0	680	0	1			0
0.17	77	0.62	140	680	0	680	0	2			0
0.17	77	0.57	150	270	240	510	260	6	−0.20	−0.05	4
1.9	44	0.55	150	150	0	150	0	9	0.67	0.40	9
1.9	70	0.55	150	150	0	150	0	11	0.76	0.63	11
1.9	88	0.55	150	150	2	150	2	13	0.84	0.66	12
7.8	44	0.54	160	150	2	150	2	12	0.81	0.66	12
7.8	70	0.54	160	150	1	150	1	12	0.84	0.79	12
7.8	88	0.54	160	150	1	150	1	12	0.77	0.82	11
30	8	0.69	120	120	0	120	0	5			0
30	32	0.69	120	120	0	120	0	2			0
30	56	0.69	120	120	2	120	2	4			0
30	76	0.69	120	120	1	120	1	5			0
30	77	0.69	120	120	1	120	1	11			0
30	77	0.30	270	690	300	810	2	7			0
37	16	0.55	150	150	2	250	220	11	0.33	0.24	4
37	44	0.55	150	180	90	180	90	11	0.74	0.64	3
37	52	0.55	150	140	34	290	250	12	0.80	0.66	3
37	70	0.55	150	150	1	180	130	17	0.88	0.80	7
37	70	0.55	310	120	39	580	240	14	0.78	0.69	1
37	88	0.26	310	300	4	530	280	9	0.30	0.23	6
37	140	0.55	150	150	2	170	75	13	0.01	0.30	6
45	75	0.68	120	120	2	120	2	3			0
45	76	0.68	120	120	0	120	0	4			0
68	44	0.54	160	170	150	620	320	7			0
68	52	0.54	160	130	130	610	240	10			0
68	70	0.54	160	190	180	630	170	11	0.36	0.25	3
68	88	0.59	140	170	200	700	1	7			0
120	9	0.68	130	120	1	120	1	3	−0.73	−0.74	1
120	29	0.88	97	300	0	300	0	1			0
120	29	0.68	130	120	0	120	0	2			0
120	49	0.68	130	110	25	120	0	4			0
120	64	0.62	140	110	36	110	36	2			0
120	65	0.62	140	120	0	120	0	5			0
120	65	0.26	320	280	76	250	100	11	−0.04	−0.07	1
120	66	0.26	320	220	150	220	140	3			0
120	67	0.88	97	300	0	300	0	2			0
120	67	0.68	130	120	2	120	2	2			0
120	67	0.62	140	130	11	130	11	2			0
120	67	0.26	320	300	0	300	0	3			0

[a]Freq is the fundamental resonance frequency of the air column. Lower and Upper are the averaged measured frequency by the lower and upper microphone at the maximum amplitude, respectively, and std(L) and std(U) are their standard deviation, respectively. Number 1 is the number of successful experiments. cL and cU show the correlation coefficient between the synthetic and the measured waveform for the lower and upper microphone, respectively. Number 2 is the number of experiments in which the aperture growth velocity is successfully measured.

tension to those of silicate melts [e.g., *Namiki and Manga*, 2008]. By varying the water content of the syrup, we change its viscosity, η_{liq}, from 10^{-3} Pa s (water) to 120 Pa s, which partially covers the viscosity range of the basaltic magma $1 < \eta_m < 1000$ Pa s [e.g., *Spera*, 2000]. The shear viscosity of the syrup is measured with a concentric cylinder viscometer (Brookfield). The surface tension σ of aqueous sugar solution without contamination is similar to that of pure water [e.g., *Lindfors*, 1924], and we estimate the surface tension of syrup as 0.07 N m^{-1}. The density of syrup depends on the concentration of sugar and is in the range of $1000 < \rho_{liq} < 1450$ kg m^{-3}.

[21] We perform experiments by varying the viscosity of the syrup and the final bubble volume. In order to vary the final volume of the bubble, we change both the volume and the pressure of the pool. We regard the pressure in the pool does not affect the pressure inside the bubble when it bursts. This is because the ascending distance of the bubble in the liquid column is sufficiently long for the bubble to expand. We estimate the pressure inside the bubble in syrup whose viscosity is 120 Pa s by calculating the volume of the ascending bubble from a two-dimensional side view assuming a spheroidal shape. We find that the pressure inside the bubbles is the same irrespective of the pool pressure.

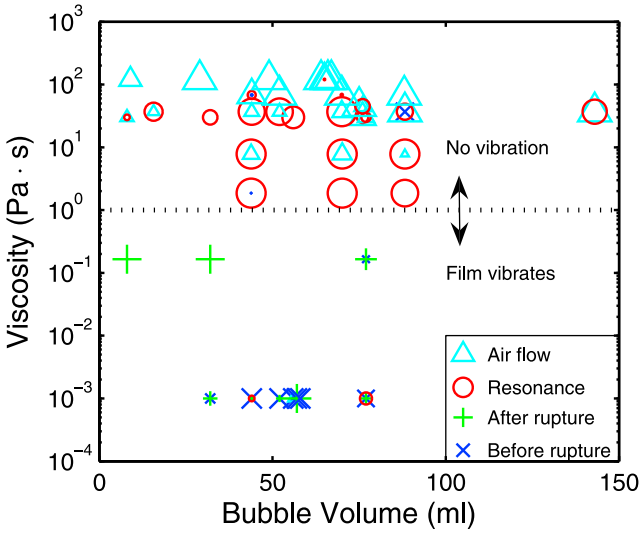

Figure 2. Regime diagram of the measured airwave excited by the bubble. The symbols denoted as "Before rupture" and "After rupture" indicate that a prominent airwave is observed before an aperture appears on the bubble film and after the bubble disappears, respectively. "Resonance" indicates that airwaves with frequency close to the fundamental mode of air column resonance are excited just after the bubble film ruptures. "Air flow" indicates a low-frequency pressure fluctuation that is usually detected only by the lower microphone. The size of the symbol represents the percentage of the experiments in which the corresponding phenomenon is observed. Visual observation shows that the bubble film does not vibrate when the liquid viscosity is larger than 1 Pa s.

Based on the discussion in section 5.1, the estimated bubble film just before the bubble bursting is less than 1 mm. Such a thin film may not be capable of supporting a significant overpressure inside a bubble. We thus calculate the final bubble volume under the assumption that the pressure inside the bubble is equivalent to the atmospheric pressure, 10^5 Pa. In reality, there should be a small overpressure inside the bubble due to the surface tension which could vary if the bubbles have different curvatures. Experiments are performed at room temperature 20–27°C, which changes the sound velocity in air as 343–348 m s^{-1}. Table 1 summarizes the conditions and the number of experiments.

4. Experimental Results

4.1. Regime Diagram

[22] Figure 2 summarizes the parameter regime and the results of the experiments. Different symbols indicate the types of airwaves. The marker sizes indicate the percentage of experiments in which the phenomena described are observed.

[23] We find that the bubble behavior and airwaves strongly depend on the liquid viscosity. When the liquid viscosity is small (<1 Pa s), in general, the bubble film vibrates before rupturing. The sequence of film rupture is as follows. An aperture appears on the bubble film, which then grows to the end of the film, and finally the bubble disappears. The prominent airwave appears before an aperture appears or after the bubble disappears, which is denoted by crosses and pluses, respectively, in Figure 2. Details of these features are described in sections 4.2 and 4.3.

[24] On the other hand, bubbles in a viscous fluid (>1 Pa s) do not vibrates. Bubble films rupture in the following sequence. An aperture appears on the bubble film and grows. The growth of the aperture halts at a certain radius, and the bubble film then falls as a result of its own weight. When the aperture appears on the bubble film, the amplitude of the airwave increases. The observed frequency of this wave is close to the fundamental mode of the air column resonance. This feature is denoted by circles in Figure 2. In some experiments, a fluctuation of air pressure with low frequency is observed, which is denoted by triangles in Figure 2. Details are described in section 4.4.

4.2. Experiments With Water (10^{-3} Pa s)

[25] Figure 3 is a typical experiment with a low-viscosity liquid (see Animation 1).[1] Experiments are performed with water with a viscosity of 10^{-3} Pa s. The bubble volume injected into the liquid column is 44 mL; the fundamental and the second-order resonance frequency of the air column are 150 and 460 Hz, respectively.

[26] Figure 3a shows the snapshots of the bubble behavior. At 0.074 s, the bubble is located under the liquid surface. The outline of the bubble under the water is denoted by dashed curve and the liquid surface is denoted by the arrow. A schematic diagram (Figure 3b, step i) shows this regime. At 0.094 s, the bubble cap reaches the surface and excites waves on the liquid surface as shown in Figure 3b, step ii. The outline of the bubble film is denoted by the orange curve. Until 0.154 s, the bubble ascends and the liquid between the bubble and the acrylic wall drains. After the bubble ascent stops, its spherical shape changes to a cylindrical one, and the upper bubble film becomes flat (0.174–0.214 s). On the flat bubble film, there exist some waves which may be reflections of a wave excited by the bubble cap (Figure 3b, step iii). In this experiment, during the stage in which the hemispherical bubble film becomes flat, it vibrates (0.214 s) and releases a droplet, shown by the orange circle at 0.234 s (Figure 3b, step v). At 0.254 s, an aperture appears on the flat bubble film and grows (vi), which is usually called a "film rupture" or "bubble bursting." At 0.274 s, the debris of the film still remains as an elongated droplet shown by the orange circle, then at 0.294 s, the bubble disappears (Figure 3b, step vii).

[27] Airwaves measured by the microphones in the air column correlate with some of these bubble behaviors. Figure 3b is the measured airwave by microphones in which a linear trend is subtracted. When the bubble cap reaches the liquid surface (Figure 3b, step ii), the amplitude of the airwave becomes large. The amplitude decreases during the stage in which the bubble cap is becoming larger. When the flat bubble film vibrates, the high-frequency wave overlaps (Figure 3b, step v). The appearance of the aperture on the bubble film indicated by the thick line does not significantly alter the air waveform (Figure 3b, step vi). Figure 3c shows the spectrogram of the measured airwave shown by the blue curve in Figure 3b. When the bubble reaches the surface

[1] Animations are available in the HTML.

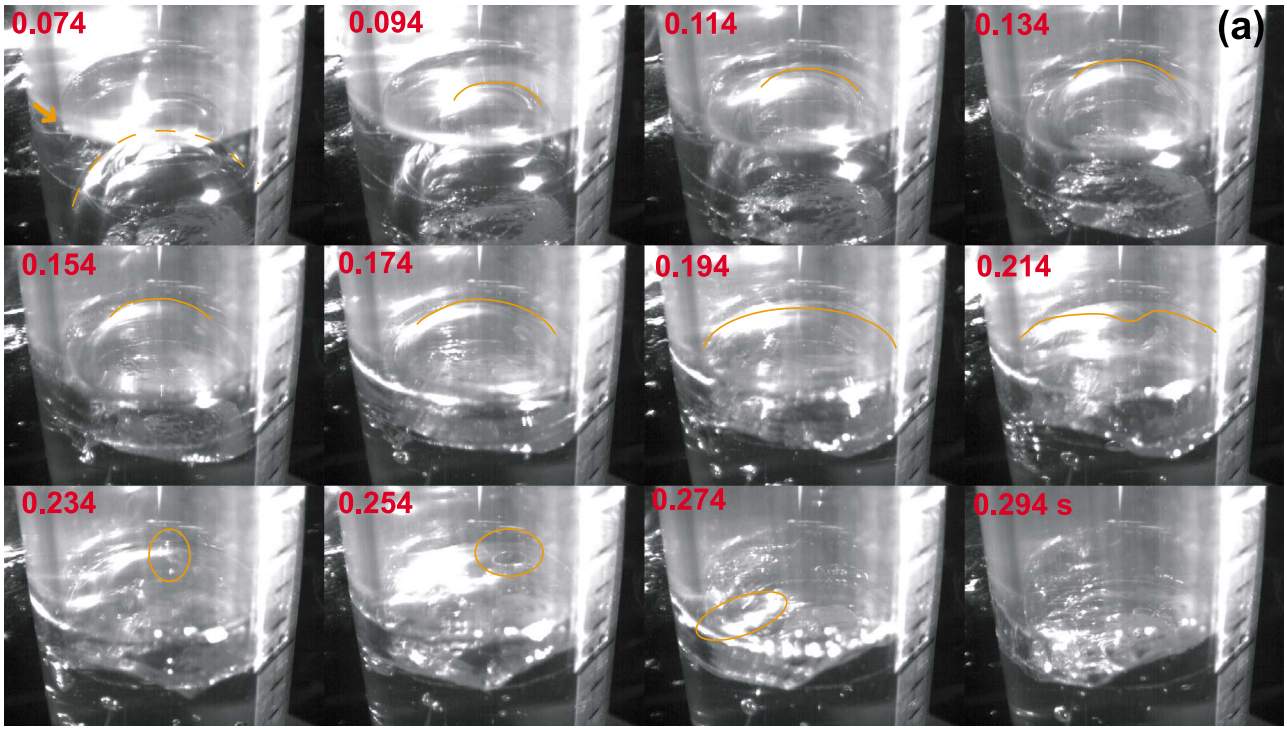

Figure 3. An experiment in water (viscosity 10^{-3} Pa s) for a bubble volume of 44 mL, with an air column length of 0.55 m whose fundamental and second-order resonance frequencies are 150 and 460 Hz, respectively. (a) Snapshots of the bubble. The numbers at the top left indicate the elapsed time in seconds from the reference time. Orange curves indicate the outline of the bubble, and orange circles show the loci of prominent phenomena. At 0.254 s, an aperture appears on the bubble film. The inner diameter of the acrylic pipe is 56 mm. A movie is provided as Animation 1. (b) Measured airwaves with schematic diagrams showing the sequence of bubble behavior as steps i–vii. Blue and green curves indicate the measurements by the lower and upper microphones, respectively. Vertical black lines show the timing at which the behavior of the bubble changes. The thick line indicates the timing immediately before the appearance of the aperture on the bubble film. Inset is the close-up view of the airwave when the aperture appears on the film. Dashed and dotted lines indicate the times at which the airwave arrives at the lower and upper microphones, respectively, after the aperture appears on the film. The superimposed red line is the synthetic waveform calculated by equation (10). (c) Spectrogram of the blue curve in Figure 3b. Red corresponds to a larger intensity.

(0.1 s), an airwave with a frequency of 150 Hz is excited. This frequency is the same as that of the fundamental mode of the air column resonance. Around 0.25 s, an airwave with a higher frequency (~10^3 Hz) is excited. The frequency increases gradually as a function of time. One possible explanation is that the bubble film vibration generates airwaves just before an aperture appears on the bubble film. In the bubble film vibration, the bubble film should become thinner as a result of drainage as time elapses. Equation (4) shows that the thinner film generates higher-frequency waves, which explains the observed result as shown in Figure 3c. It is not obvious whether the signal associated with Helmholtz resonator is observed. If the airwave generated by a Helmholtz resonator is observed, its frequency should increase as a function of time from several hundred hertz to a thousand hertz. The frequency of the Helmholtz resonator depends on the aperture radius, as shown in equation (5), and the observed aperture radius increases as a function of the elapsed time. However, the timescale of aperture growth 0.02 s is not long enough compared to the inverse of the Helmholtz resonator frequency, and as a consequence a standing wave inside the bubble may not develop. On the other hand, the signal associated with the instantaneous removal of the bubble film, 6900 Hz from equation (6), is not observed.

[28] We perform 26 experiments with water, as denoted in Table 1 and Figure 2. In 88% of the experiments, prominent airwaves are excited before the aperture appears on the film, suggesting that the waves originated with the bubble film excite the airwaves. We classify this feature as "before rupture" and denote by crosses in Figure 2.

[29] Details of the bubble behavior and the resulting airwave vary among experiments. In some experiments, short-wavelength ripples appear on a flat bubble film with a wavelength of around 1 mm, as shown in Figure 4a. This wave could be a surface wave. When this wave appears, the high-frequency component of the airwave (several 100 Hz) is excited (Figures 4b and 4c). Sometimes, the amplitude of the airwave becomes large again after the bubble film disappears as shown in Figure 4b. This feature is denoted by

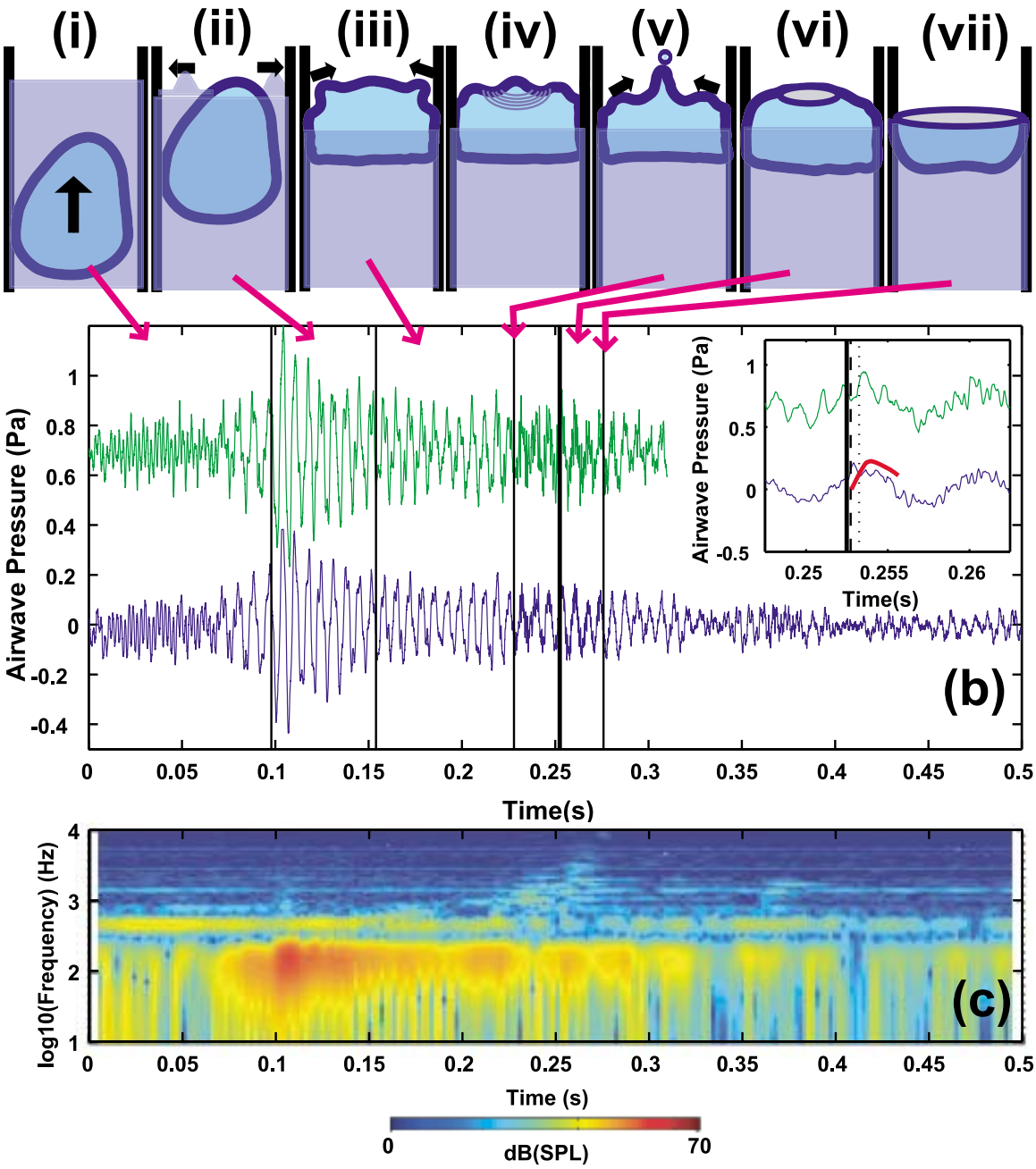

Figure 3. (continued)

pluses in Figure 2. In some experiments, two apertures appear on the film during the film rupture.

[30] In spite of diversity of the observed phenomena, the most prominent frequency of the observed airwave is always 150 Hz, which is the fundamental resonance frequency of the air column throughout the sequence shown in Figures 3 and 4. This fact suggests that whenever the frequency matches with the resonance frequency of the air column, the frequency can be amplified. Indeed, experiments with a longer air column (700 mm) above water produce waves with lower fundamental frequency (120 Hz) and their higher modes.

4.3. Experiments With Intermediate Liquid Viscosity (0.17 Pa s)

[31] Figure 5 shows a case in which the liquid viscosity is 0.17 Pa s (see Animation 2). The cap of the ascending bubble in the liquid column reaches the surface at around 0.15 s (Figure 5a, step i). The bubble cap is denoted by orange curves. Differently from the case with water, waves on the liquid surface are not observed. The bubble continues to ascend, and the cap expands (Figure 5a, step ii). At around 0.2 s, the bubble ascent stops, and the hemispherical cap becomes flat (Figure 5a, step iii). In some experiments,

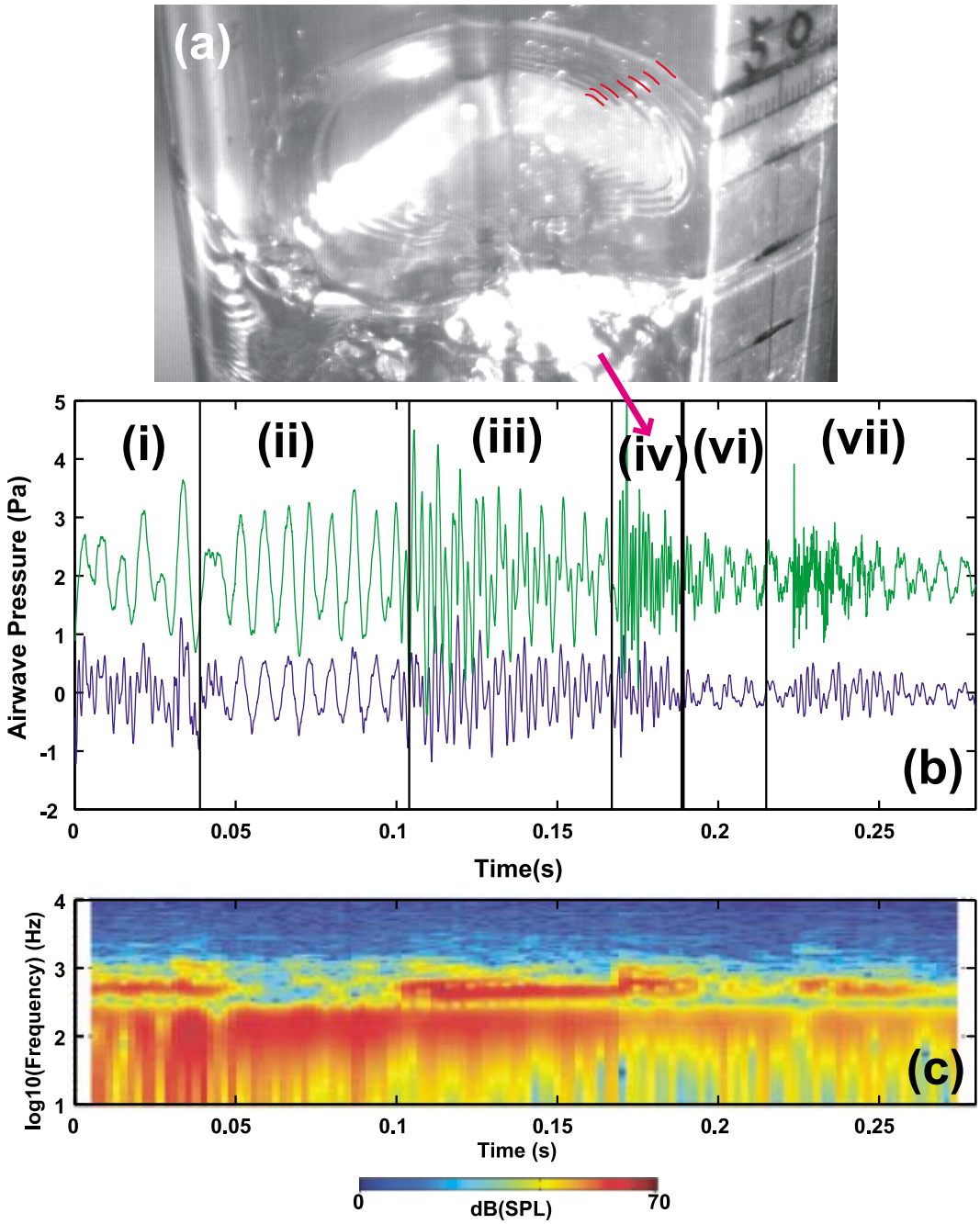

Figure 4. Another experiment in water for a bubble volume of 77 mL, with an air column length of 0.55 m whose fundamental and second-order resonance frequency is 150 and 460 Hz, respectively. (a) Snap shot during the experiment, showing the wave at the flat film denoted by red curves. (b and c) Same as in Figures 3b and 3c. Steps i–vii are the regimes described in Figure 3b.

the bubble pulsates at this stage. At 0.245 s, an aperture appears on the bubble film and spreads (Figure 5a, step iv). The edge of the aperture reaches the acrylic wall at around 0.28 s, and then the bubble disappears (Figure 5a, step v). Differently from the case with water, the amplitude of the airwave increases significantly after the bubble disappears (Figure 5b). When the bubble reaches the liquid surface and an aperture appears on the film, the change of the waveform

Figure 5. An experiment in liquid (viscosity 0.17 Pa s), for a bubble volume of 77 mL, with an air column length of 0.57 m whose fundamental and second-order resonance frequencies are 150 and 450 Hz, respectively. (a, b, and c) Same as Figures 3a, 3b, and 3c. In Figure 5a orange curves at 0.128–0.228 s indicate the bubble cap. After 0.248 s, the orange curves indicate the edge of the aperture on the film. A movie is provided as Animation 2.

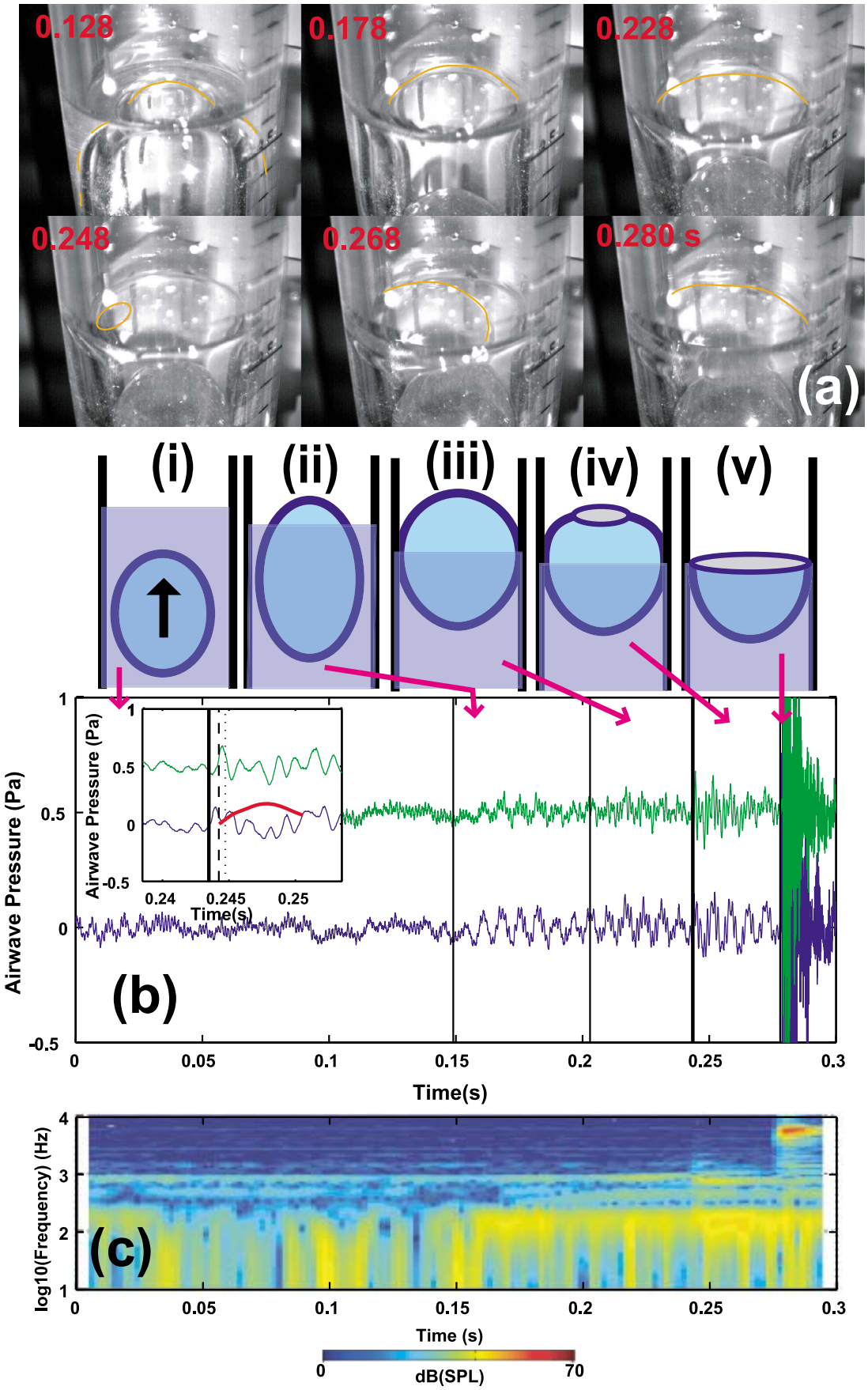
0.128
0.178
0.228
0.248
0.268
0.280 s
(a)
(i)
(ii)
(iii)
(iv)
(v)
Airwave Pressure (Pa)
Time(s)
(b)
log10(Frequency) (Hz)
(c)
Time (s)
dB(SPL)
0
70

Figure 5

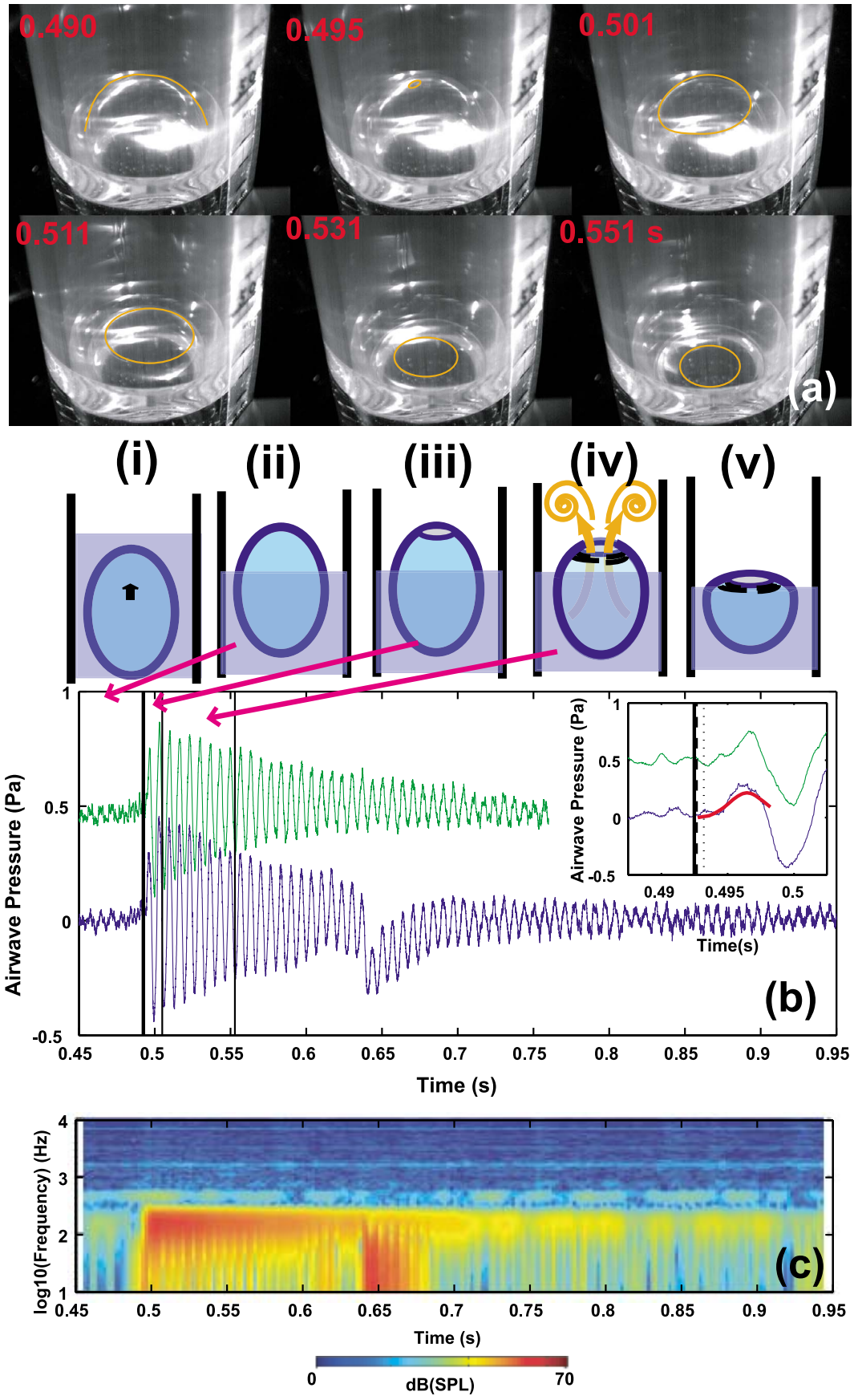
0.490
0.495
0.501
0.511
0.531
0.551 s
(a)
(i)
(ii)
(iii)
(iv)
(v)
Airwave Pressure (Pa)
Time (s)
Time(s)
(b)
log10(Frequency) (Hz)
(c)
dB(SPL)

Figure 6

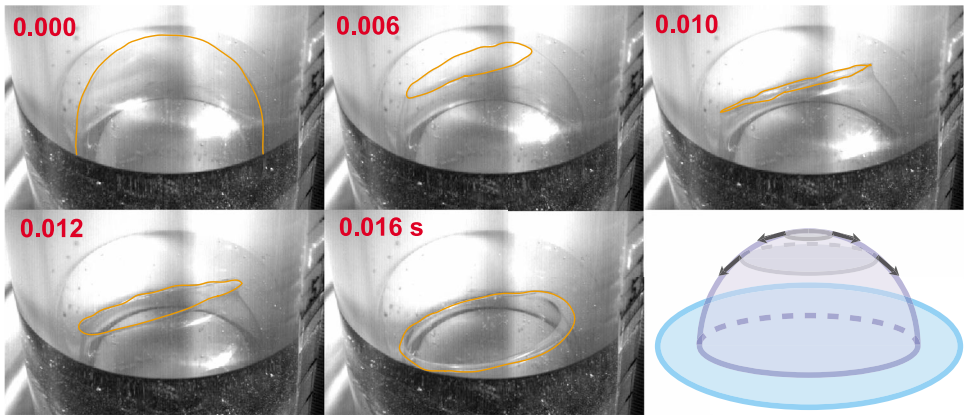

Figure 7. A sequence of images during the experiment in which the aperture edge turns outward. The liquid viscosity is 1.9 Pa s, the bubble volume is 88 mL, and the air column length is 0.55 m. The numbers at top left indicate the time after the aperture appears on the film. The orange curves indicate the outline of the bubble (0.000 s) and the edge of the aperture on the film. The schematic diagram shows direction of surface tension and how it changes with the aperture growth.

of air pressure is small compared to the case for water. We classify this feature as "after rupture" and denote it by pluses in Figure 2. The measured frequency of the airwave by the microphone near the bubble during which the bubble exists at the surface is 140 Hz and is close to the fundamental resonance frequency of the air column 150 Hz rather than that of the bubble film vibration. The frequency of the airwave after the bubble disappears is around 6000 Hz whose source is unknown (Figure 5c). The maximum number of apertures is three, which we observed in one experiment for this viscosity.

4.4. Experiments With High-Viscosity Liquid (>1 Pa s)

[32] When the liquid viscosity is larger than 1 Pa s, the behavior of the bubble is quite different from the case for a low-viscosity liquid. Figure 6a and steps i–v in Figure 6b, shows the sequence of bubble bursting (Animation 3). When the cap of the bubble protrudes over the liquid surface, neither the liquid surface nor the bubble film vibrates (Figure 6b, steps i and ii). In some experiments, we observed waves with wavelengths of less than 1 mm which travels on the bubble film, but their amplitude is not large enough to change the bubble shape. An aperture appears on the film (0.495 s), but its growth stops at a certain radius (Figure 6b, step iii). The bubble deflates by its own weight (Figure 6b, step iv). Finally, the bubble film reaches the liquid surface (0.551 s). The liquid between the bubble and acrylic wall descends, and the bubble disappears (Figure 6b, step v).

[33] Differently from the case with a low-viscosity liquid, the amplitude of the airwaves significantly increases when the aperture appears on the bubble film, as shown in Figure 6b at 0.493 s. The frequency of the excited airwave is 150 Hz, as shown in Figure 6c, which is the same as that of the fundamental mode of the air column resonance. We classify this as "resonance" and indicate it by circles in Figure 2. At around 0.65 s, only the lower microphone detects the low-frequency pressure fluctuation, and we interpret this as an air flow generated by the deflation of the bubble, as illustrated in Figure 6a, step iv. The details are discussed in section 5.4. When the low-frequency air pressure fluctuation is observed, we classify this as "air flow" and indicate it by triangles in Figure 2.

[34] For the case of liquid viscosity with 1.9 and 7.8 Pa s, two or three apertures are observed in some experiments. In experiments with more viscous liquids, we sometimes do not observe an aperture, but the bubble deflates, and this deflation is accompanied by air pressure fluctuation. We interpret that an aperture which is too small to be observed forms on the bubble film, and the gas in the bubble leaks from this aperture. In such a case, we use the timing of bubble deflation as the beginning of the bubble film rupture. In experiments with liquid viscosity of 1.9 Pa s, the edge of the growing aperture turns outward, as shown in Figure 7. This may be because the direction of the surface tension changes as the aperture grows, as shown in the schematic diagram in Figure 7.

4.5. Effect of the Boundary Condition

[35] Figure 8 shows the experiment with the same conditions as in Figure 6, but the upper end of the air column is covered with plastic wrap, which act as a closed end. The boundary condition affects the resonance frequency of the air column. The frequency of the air column resonance under the fundamental mode is 310 Hz, which is twice that in Figure 6.

Figure 6. An experiment in viscous liquid (viscosity 37 Pa s), for a bubble volume of 70 mL, with the air column length of 0.55 m whose fundamental and second-order resonance frequencies are 150 and 460 Hz, respectively. (a, b, and c) Same as Figures 3a, 3b, and 3c. In Figure 6a before the aperture appears (0.490 s) the orange curve indicates the outline of the bubble. After the aperture appears, the orange circles indicate the edge of the aperture on the film. Vertical black lines in Figure 6b indicate the timing just before an aperture appears on the film, the end of the aperture growth, and arrival of the bubble film to the surface. A movie is provided as Animation 3.

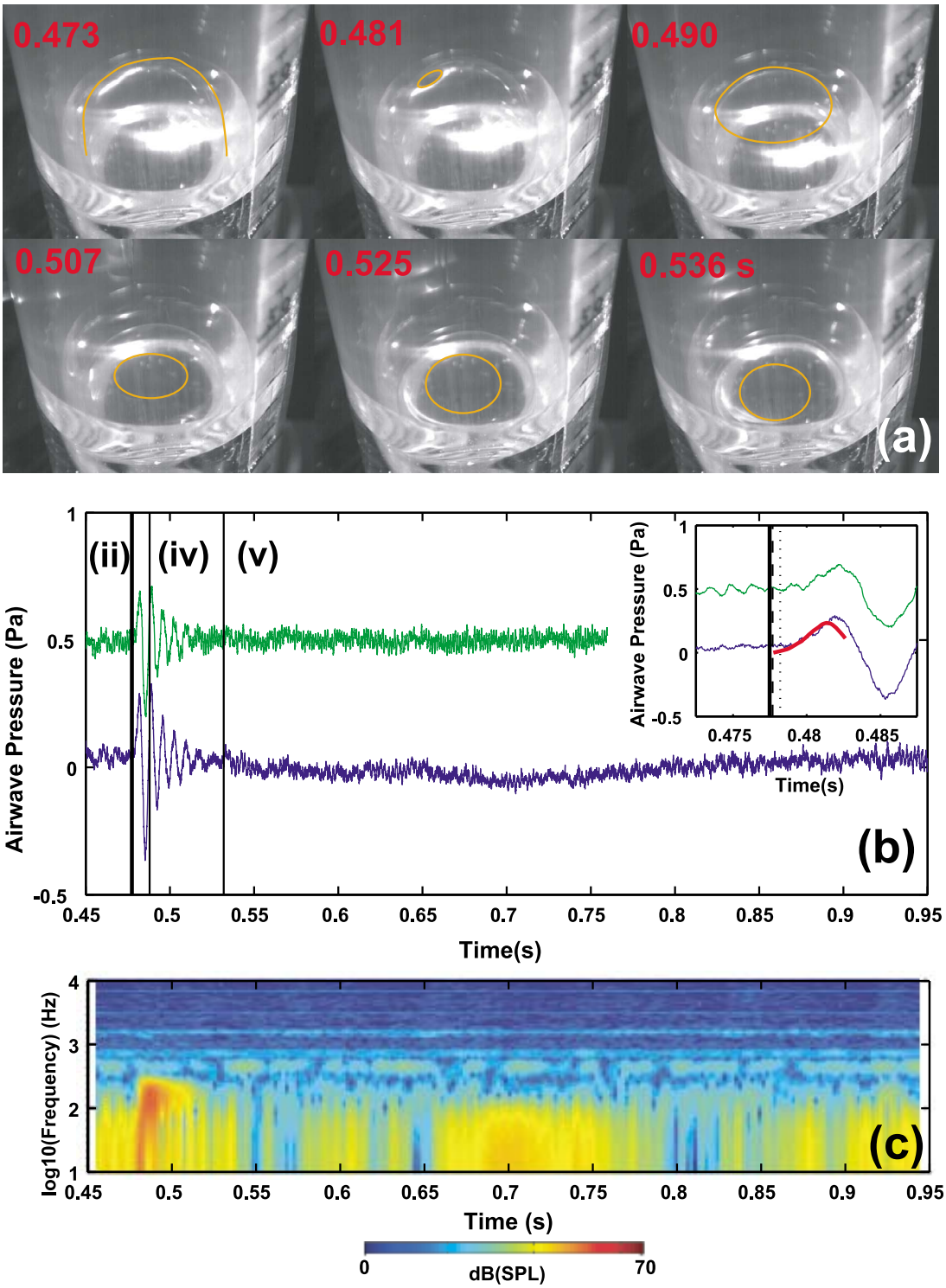

Figure 8. Same experiment as in Figure 6, but here the upper end of the air column is covered with a plastic wrap which forms a closed end. The fundamental and second-order resonance frequencies of the air column are 310 and 630 Hz, respectively. (a, b, and c) Same as Figures 6a, 6b, and 6c. Steps ii, iv, and v are the regimes described in Figure 6.

[36] The observed waveform of the air pressure in Figure 8b is different from the case with an open end shown in Figure 6b, although the sequence of bubble bursting (Figure 8a) is quite similar to the case with an open end (Figure 6a). An airwave is excited when the aperture appears on the bubble film at around 0.48 s; its frequency is 140 Hz which is approximately one half of the resonance frequency. The resonance, however, does not continue for a long time.

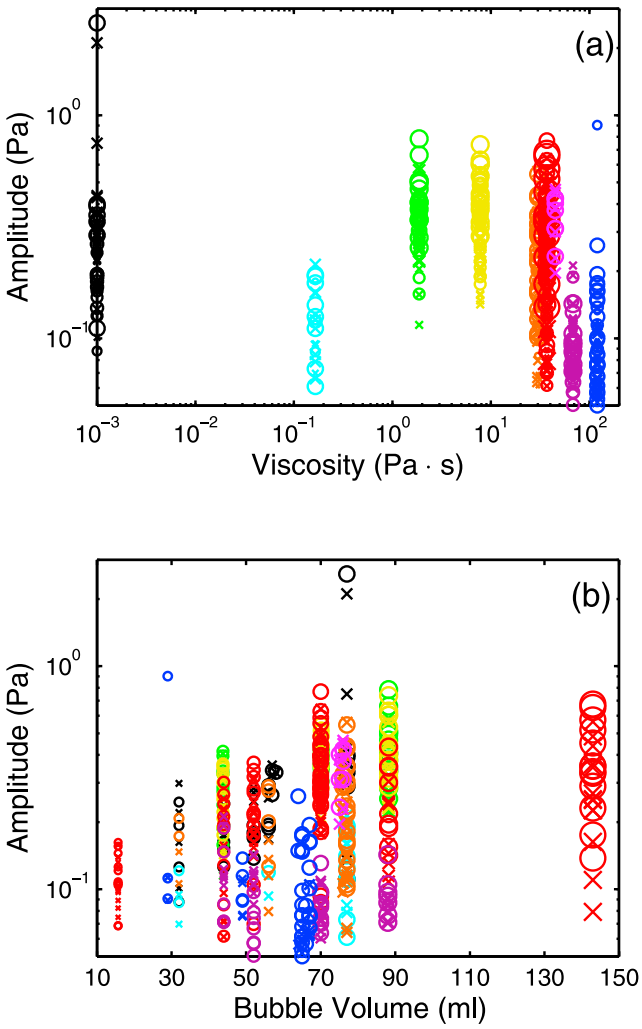

Figure 9. Measured amplitudes of the airwaves after the aperture on the bubble film appear within two cycles of the air column resonance. (a) The liquid viscosity dependence and (b) the bubble volume dependence. Each symbol indicates the result of an experiment. Circles and crosses show the amplitude measured by the lower and upper microphones, respectively. The color and size of symbols represent the liquid viscosity and the bubble volume, respectively. The experiments with a smaller bubble volume are shown by smaller symbols. We use same color and size of symbols in Figures 10 and 14–17.

4.6. Amplitude of the Airwave

[37] Figures 9a and 9b show the amplitude of the airwave measured by the microphones as functions of the liquid viscosity and the bubble volume dependence, respectively. In order to calculate the amplitude, we use the time window from the time in which the aperture appears on the bubble film until the time when the air column oscillates two cycles at the fundamental mode of resonance. Figure 9 shows that the measured amplitude of the airwave varies among experiments with same conditions. We here focus on the average amplitudes among the same viscosity or volume. This is because the apertures on the bubble do not necessarily appear on the top of the bubble. When an aperture appears on the side of a bubble film, the airwave surface inclines with respect to the microphones and observed amplitudes may be reduced. In addition, the initial overpressure inside the bubble may vary among experiments.

[38] In general, when the liquid viscosity is within the range of $1 < \eta_{liq} < 50$ Pa s, large-amplitude airwaves are observed comparing the experiments with same volume. On the other hand, larger-volume bubbles give rise to larger-amplitude airwaves.

4.7. Measurement of the Aperture Growth

[39] In the experiments reported above, we find that bubble bursting is initiated by an aperture appearing on the film. Here, we measure the time-dependent aperture radius. The aperture growth cannot always be measured successfully. This is because in some cases the aperture becomes out of focus since it is difficult to predict the exact location in which the aperture forms. The number of experiments in which we successfully measured the aperture growth is listed in the last column of Table 1.

[40] Figure 10a shows the time evolution of the aperture radius on the bubble film. The color indicates the difference of liquid viscosity. Figure 10a shows that the aperture on the film for a less viscous liquid, <1 Pa s, denoted by black and light blue lines, grows at a constant velocity. On the other hand, for a more viscous liquid, the aperture growth first accelerates, then decelerates, and finally stops at a certain radius. After the aperture growth halts, the bubble deflates as shown in Figure 6.

[41] Figure 10b shows the final aperture radius. Among the experiments whose viscosity is >1 Pa s, a smaller liquid viscosity gives rise to a larger final aperture radius. Figure 10c shows the aperture growth velocity. When the liquid viscosity is large, the aperture grows slowly.

5. Discussion

[42] Experiments show that when the liquid viscosity is low (<1 Pa s), the bubble vibrates before the bursting. Airwaves are observed before an aperture appears on the bubble film or after the bubble disappears. On the other hand, when the liquid viscosity is high (>1 Pa s), the amplitude of the airwave increases immediately after the aperture appears on the bubble film, suggesting that the overpressure inside the bubble which is exposed to the atmosphere through the aperture excites the airwave. If the aperture is the source of the airwave which grows as a function of time, the source size also increases as a function of time. Here, we first discuss the mechanism of aperture growth and then construct a model of an airwave excited by the aperture growth.

5.1. Mechanism of the Aperture Growth

[43] From Figure 10, we find that the liquid viscosity changes the characteristics of the aperture growth. For a less viscous liquid (<1 Pa s), the aperture grows at an approximately constant velocity. On the other hand, for a more viscous liquid (>1 Pa s), the aperture growth first accelerates then decelerates and finally halts. This result suggests that the aperture growth mechanism depends on the liquid viscosity.

[44] Two mechanisms of film rupture have been reported. Under the classic theory, the aperture on the film grows at a constant velocity [*Taylor*, 1959; *Culick*, 1960]

$$v_{\mathrm{i}} = \sqrt{\frac{2\sigma}{\rho_{\mathrm{liq}} h}}. \tag{7}$$

In this case, the retracting liquid which have consisted the film is collected into the rim of the aperture. Here, the surface tension force balances the inertia force. We call this the inviscid model.

[45] Recently, exponential acceleration of the aperture growth was reported for a case with large liquid viscosity [*Debregeas et al.*, 1995, 1998],

$$v_{\mathrm{v}} = \frac{\sigma}{\eta_{\mathrm{liq}} h} R, \tag{8}$$

where R is the aperture radius and depends on time t,

$$R(t) = R_0 \exp\left(\frac{\sigma}{\eta_{\mathrm{liq}} h} t\right). \tag{9}$$

In this case, the retracting fluid causes the film to thicken uniformly instead of creating a rim. One explanation of film thickening is viscoelasticity. Another explanation is that the Stokes length, a typical length scale of the velocity gradient within the film, is longer than the lateral extent of the film [*Brenner and Gueyffier*, 1999]. The upper limit of the velocity should correspond with the one calculated from equation (7). We call this the viscous model.

[46] In order to compare the measured aperture growth in our experiments with these two models, we calculate the correlation coefficient between the measurement and the two models. Figure 11a shows that in a low-viscosity liquid, the correlation coefficient is higher for an inviscid model compared to a viscous model, and vice versa for a high-viscosity liquid. This result is qualitatively consistent with our observation, in which the aperture grows at a constant velocity for a low-viscosity liquid (<1 Pa s), whereas the aperture growth halts at a certain radius for a high-viscosity liquid (>1 Pa s). When the liquid viscosity is 1.9 Pa s, the aperture growth seems to stop at a certain radius, but the inviscid model gives a better fit. We here note that the difference of the calculated correlation coefficient between two models is fairly small, such that it is difficult to define the exact threshold viscosity at which the mechanism of the aperture growth changes.

[47] We can also calculate the film thickness using equations (7) and (8). Figure 11b shows the calculated bubble film thickness using the two models. As mentioned above, we consider that at low and high viscosities, inviscid and viscous models, respectively, are more applicable. From Figure 11b, this indicates that the film thickness is in the range of $1 < h < 100$ μm, and that it decreases with viscosity. We interpret that a bubble in a high-viscosity liquid has a sufficiently long time at the surface before the aperture appears, thus allowing more liquid to drain.

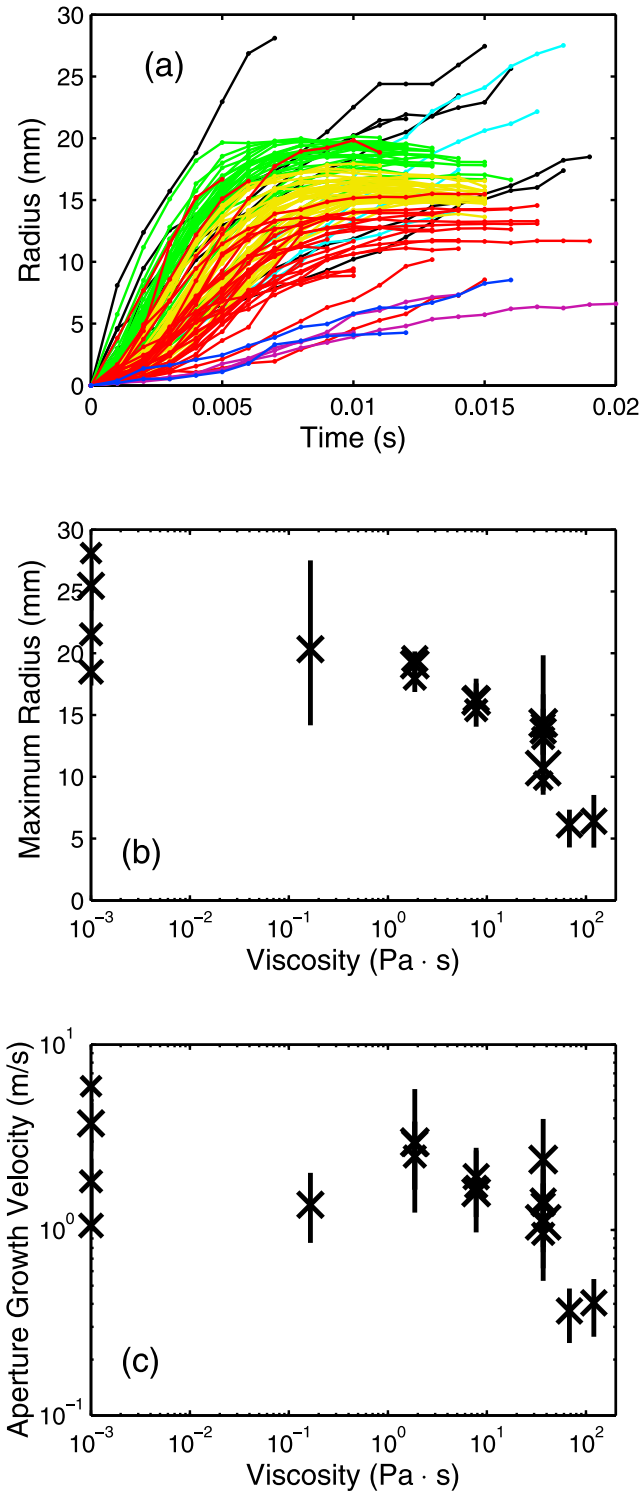

Figure 10. (a) Time evolution of the aperture radius. The color indicates differences of liquid viscosity and is the same as in Figure 9. (b) Observed maximum aperture radius in Figure 10a as a function of liquid viscosity. Crosses indicate the averaged values for each bubble volume. The size of the symbols corresponds to the bubble volume. Vertical lines indicate the observed range of radius. (c) Mean velocity of the aperture growth as a function of the liquid viscosity. The velocity is calculated within the time span from the beginning of the aperture growth until the velocity becomes the maximum. Symbols are the same as in Figure 10b.

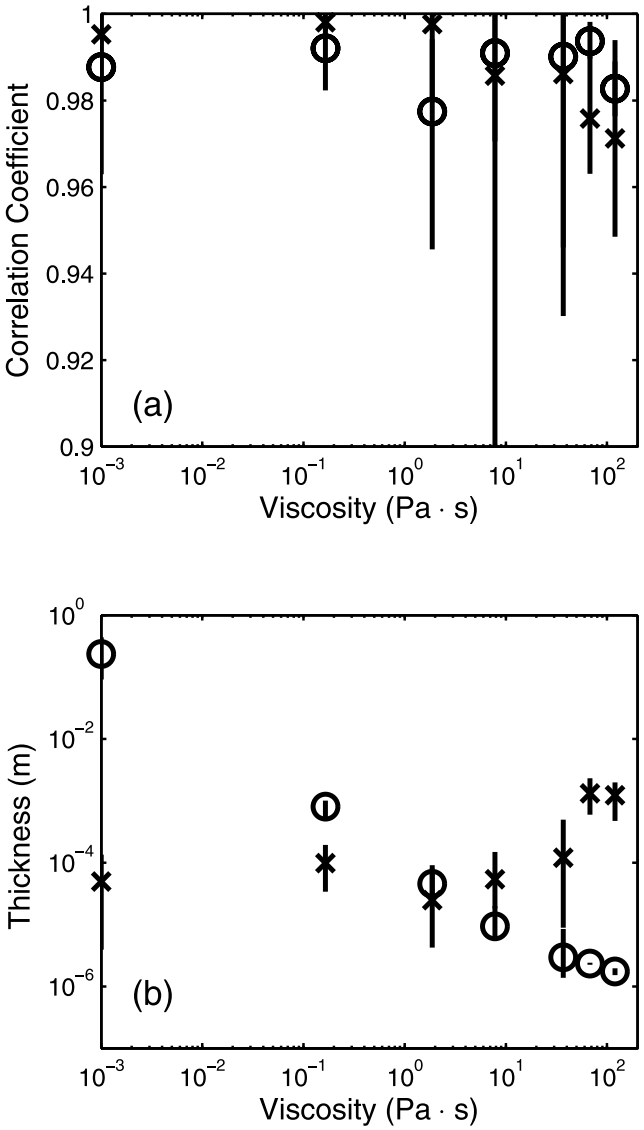

Figure 11. (a) Calculated correlation coefficient between the observed aperture growth shown in Figure 10a and the two models. Crosses are for the inviscid model (equation (7)). The time span used to calculate the correlation coefficient is chosen from the beginning of the aperture growth until the velocity becomes the maximum. Circles are for the viscous model (equation (8)). The time span is chosen such as to maximize the correlation coefficient, which corresponds to the duration in which the aperture grows at an accelerating rate. Here we plot the average of the experiments at the same viscosity, with vertical lines indicating their range (maximum and minimum). (b) Estimated bubble film thickness using the two models. The symbols are the same as in Figure 11a.

5.2. Model of the Airwave Produced by the Aperture Growth

[48] Here we make a model of the airwave generated by the aperture growth. The model is only intended to reproduce the first positive pulse of the airwave. Waveform obtained in our experiments suggest that the oscillation after the first positive pulse is the air column resonance whose waveform is sinusoidal. We discuss the air column resonance in section 5.3.

[49] We consider the situation shown in Figure 12. Gas pressure inside the bubble is $p + P_a$, where P_a is the atmospheric pressure and p is the overpressure. During bubble bursting, an aperture with a radius R appears on the bubble film. From this aperture, the pressurized gas inside the bubble is exposed to the lower atmospheric pressure. The local pressure difference in a continuous medium should excite an airwave; thus, an airwave with the amplitude p can be emitted from this aperture.

[50] If the medium does not have an intrinsic attenuation, we can estimate the maximum amplitude of the airwave measured by the microphone by using p and assuming geometrical attenuation. When the energy of the airwave emitted from the aperture is scaled as p^2 and the wave spreads in the acrylic pipe with a radius a, the amplitude of the wave measured by the microphone can be estimated as

$$p_m \sim p(t)\frac{R(t)}{a}. \tag{10}$$

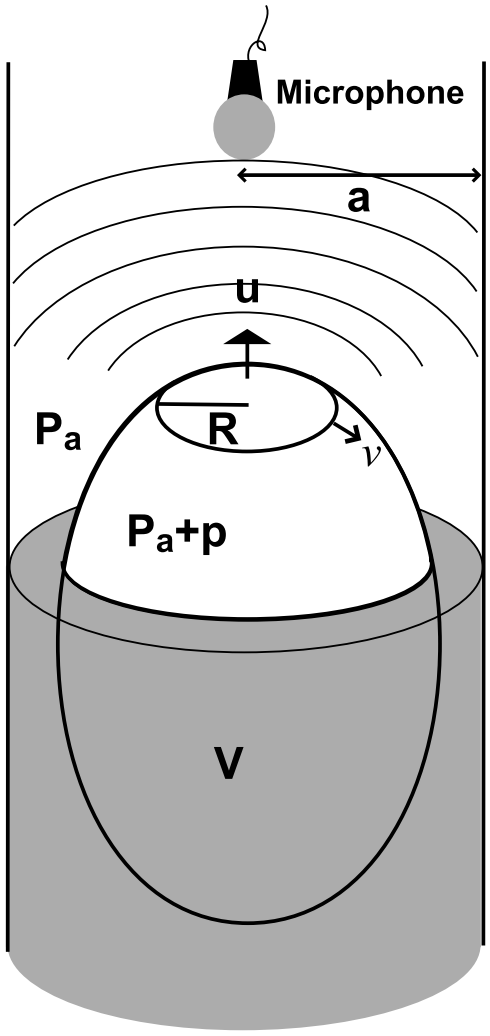

Figure 12. A schematic illustration of a bursting bubble.

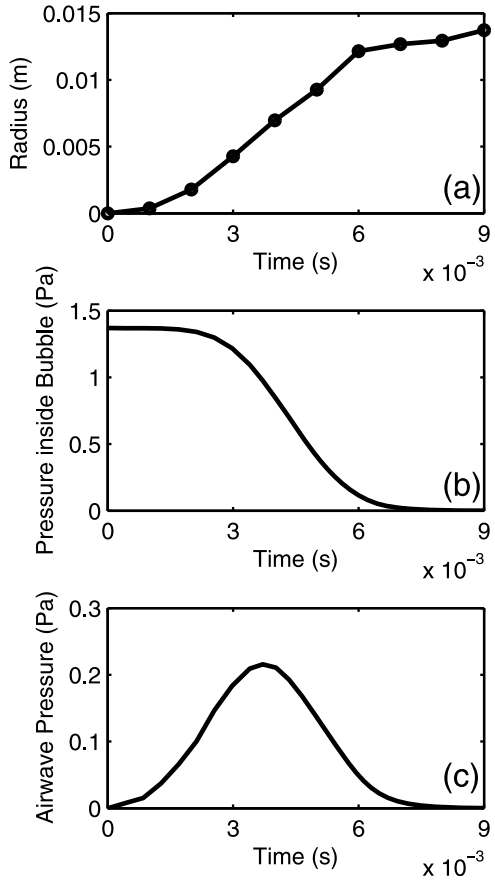

Figure 13. An example showing the method used to calculate the synthetic waveform in Figures 3, 5, 6, and 8. The parameters used here are the same as those in Figure 6. (a) Time evolution of the aperture radius on the bubble film. (b) Overpressure inside the bubble calculated by equation (13). (c) Synthetic waveform calculated by equation (10).

[51] The overpressure inside the bubble p has time dependence. When the aperture appears, the gas inside the bubble is released to the atmosphere. We here assume that this flow velocity is comparable to the particle velocity of the airwave,

$$u = \frac{p}{Z} = \frac{p}{\rho_a c_a}, \tag{11}$$

where ρ_a is the gas density under rest and Z is the acoustic impedance [e.g., *Blackstock*, 2000]. We here calculate Z from measured room temperature and the atmospheric pressure, 10^5 Pa, which are time independent.

[52] If this process occurs under constant temperature, the product of pressure and volume should be conserved because of mass conservation,

$$(P_a + p_0)V = \int_0^t (P_a + p)\pi R(t')^2 u dt' + (P_a + p)V, \tag{12}$$

where p_0 is the initial overpressure and V is the volume inside the bubble. Here, the left-hand side is the initial condition; the first term on the right-hand side is the flow exiting the aperture; and the second term indicates the mass remaining inside the bubble. Although a pressure drop may occur under the adiabatic condition, we here assume a constant temperature for the following reasons: (1) when the aperture radius is small, the pressure drop may be sufficiently slow to exchange heat between gas and a surrounding liquid, (2) the difference between the constant temperature and adiabatic assumption is insignificant when the overpressure is small relative to the atmospheric pressure $p \ll P_a$ [*Namiki and Manga*, 2005], and (3) for simplicity of calculation.

[53] Substituting equation (11) into equation (12) and neglecting the second-order term, the differential form of equation (12) is written as

$$\frac{dp}{dt} = -\frac{P_a \pi R(t)^2 p}{V \rho_a c_a}. \tag{13}$$

Using the measured aperture radius R in Figure 10, we can numerically integrate the above equation. Figure 13b shows the monotonic decrease of the overpressure inside the bubble when the aperture on the bubble film grows as in Figure 13a. In order to integrate equation (13), we assume the initial overpressure as $\sigma/2(3V/4\pi)^{1/3}$. This is one eighth of the overpressure sustained by surface tension for a spherical bubble. Figure 13c is the synthetic waveform calculated by equation (10). This waveform shows the effect of the aperture growth and the resulting pressure change inside the bubble and does not include the effect of propagation and reflection of the airwaves.

[54] The synthetic waveform is overlain on Figures 3, 5, 6, and 8. We recognize that the synthetic waveform resembles the one measured by microphones for the cases in Figures 3, 6, and 8 within the accuracy of the timing to synchronize the images and measured airwave, 10^{-3} s. We compare the measured airwave and the synthetic waveform within the duration from the onset of the aperture appearance until the amplitude of the synthetic waveform reduces to the half of the maximum. This is because, during the pressure decrease, reflection waves that are not included in the synthetic waveform may be measured.

[55] One important feature of this synthetic waveform is that the amplitude of the airwave becomes larger as the aperture growth becomes faster. This is because, when the aperture as an airwave source grows fast, the source size becomes large before the pressure inside the bubble decreases. Figure 14 shows the measured amplitude of the airwave as a function of the aperture growth velocity. In general, the faster aperture growth results in a larger amplitude of the airwave when the liquid viscosity is larger than 1 Pa · s.

[56] This model also explains the dependence of the airwave amplitude on liquid viscosity and bubble volume (Figure 9). The amplitude of the airwave becomes small when the liquid viscosity is very large, which can be interpreted to arise from the slow aperture growth (Figure 10). On the other hand, the measurement shows that larger bubbles generate larger-amplitude airwaves. This is because, when the bubble volume is large, it takes longer to reduce the overpressure inside the bubble, and the aperture then becomes large before the overpressure decreases. In Figure 9, the measured amplitude varies among experiments with same conditions. This may be because the loci of the

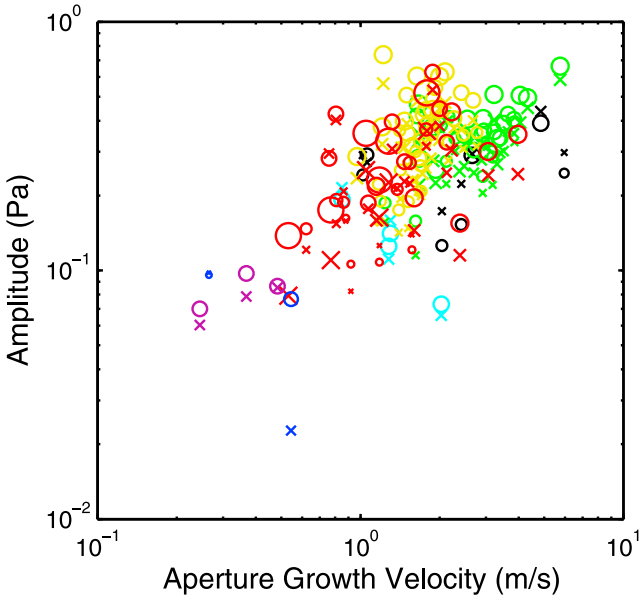

Figure 14. Measured amplitudes of the airwaves as a function of the measured aperture growth velocity. The color and size of the symbols are the same as those in Figure 9. A faster aperture growth results in a larger airwave amplitude. The velocity is determined by the inviscid (linear) model as in Figure 11.

aperture and the initial overpressure inside the bubble could vary among experiments different from our model.

[57] Figure 15 shows the calculated correlation coefficient between the synthetic and the measured air waveform. The time span used to calculate the correlation coefficient is the same as that shown in the insets of Figures 3b, 5b, 6b, and 8b. Figure 15 shows that the correlation coefficient becomes larger than 0.5 for the liquid whose viscosity is in the range of 1–40 Pa s.

[58] We interpret this result as follows. In our experiments, the airwave is excited by the aperture growth. When the liquid viscosity is very small, there are sources other than the aperture growth. Visual observation shows that the bubble film vibrates, which may excite larger-amplitude airwaves than those caused by the aperture growth. In addition, the bubbles at the top of a low-viscosity liquid have a cylindrical shape, which has a small curvature and a small overpressure, reducing the amplitude of the airwave associated with the aperture growth. We thus consider that the measured airwave is that excited by the film vibration, and, as a result, the correlation between the synthetic and measured waveform becomes low.

[59] On the other hand, when the liquid viscosity is large (>1 Pa s), the bubble film does not vibrate, and the aperture growth then becomes the dominant mechanism of airwave generation. The measured airwave represents the wave excited by the aperture growth and the correlation becomes high. When the liquid viscosity becomes even larger, the aperture growth becomes slow. The amplitude of the airwave excited by the aperture growth becomes small (Figure 14). When the amplitude becomes smaller than the noise level, the aperture growth does not excite airwaves effectively, and the microphone records only the noise, resulting in a poorer correlation between the measurement and the synthetic waveform.

5.3. When Does the Air Column Resonate?

[60] The above model explains the first pulse of the measured airwave for an intermediate liquid viscosity. The airwave generated by the aperture growth pushes the air within the acrylic pipe, above the bubble. An inertial oscillation of the air in the acrylic pipe results, owing to the compressibility of air. Our next question is when this oscillation becomes a steady air column resonance.

[61] Experiments shown in Figures 6 and 8 are performed under the same conditions except for the boundary condition in which the upper end of the air column is opened or closed. The resonance of the air column continues for a long time only when the upper end is opened. The calculated fundamental mode resonance frequency for the open-end condition is 150 Hz, which is the same as the measured one. On the other hand, the resonance frequency for the closed end is 310 Hz and is different from the measured one. Here, the first pulse of the measured waveform is similar to the synthetic one for both cases. We thus infer that when the frequency of the airwave excited by the aperture growth is close to that for the air column resonance, the airwave is amplified and the resonance continues for a long time.

[62] In order to test this hypothesis, in Figure 16 we plot the resonance duration as a function of the product of the half width of the synthetic waveform and the fundamental frequency of the air column resonance. As is evident from Figure 13c, the synthetic waveform is not sinusoidal. From

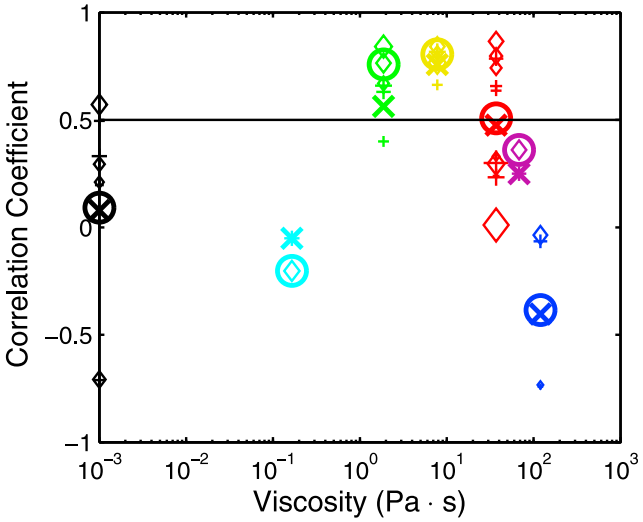

Figure 15. Correlation coefficient between the measured and synthetic waveform as a function of viscosity. The synthetic waveform is calculated by equation (10). The colors of the symbols are the same as in Figure 9. Diamonds and pluses show the mean value of the correlation coefficient between the synthetic waveform and the measured airwave for the lower and upper microphones, respectively, for the same volume and liquid viscosity. The size of symbols represents the bubble volume. Circles and crosses show the average of the value shown in diamonds and pluses, respectively, for the same liquid viscosity.

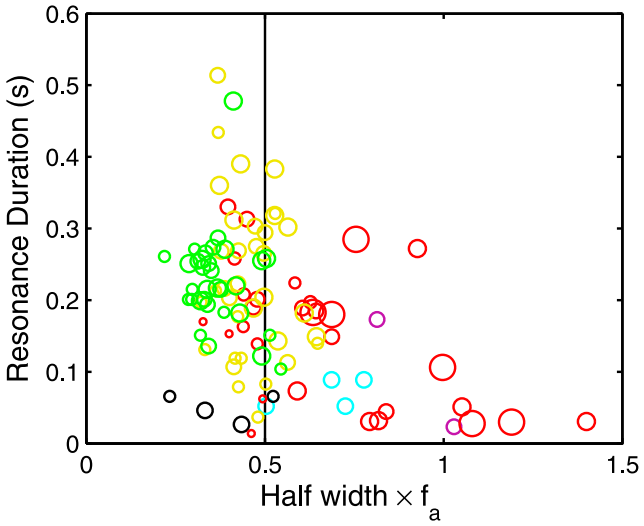

Figure 16. Observed resonance duration after the aperture appears on the bubble film as a function of the product of the half width of the synthetic waveform and the calculated frequency of the air column resonance, f_a. The color and size of the symbols are the same as in Figure 9.

Figure 6, we assume that the half width of the synthetic waveform may be approximated as the half cycle of the air column resonance. If the synthetic waveform and the resonance frequency of the air column match well, the product of these two should be plotted at around 0.5. We define the resonance duration from the time when the aperture appears on the bubble film until the time when the amplitude of the airwave becomes less than 1.3 times the amplitude before the aperture appears. The duration is calculated only when the amplitude of the airwave increases after an aperture appears on the bubble film. Figure 16 shows that when the product of the half width and the air column resonance frequency is around 0.5, the resonance continues for a long time, suggesting that the resonance is excited when the incidence waves generated by the aperture growth have a similar frequency to the resonance frequency of the air column. We thus conclude that the resonance occurs most efficiently when the eigenfrequency of the air column matches the frequency of the airwave generated by the aperture growth.

5.4. What Is "Air Flow"?

[63] During the air pressure observation with a high-viscosity liquid, we find that there is low-frequency pressure fluctuation, which sometimes does not reach the upper microphone. We named this as "air flow." Here we discuss the source mechanism of the air flow.

[64] We infer that the air flow is caused by the deflating bubble film. When there are no apertures on the bubble film, the film is sustained by the pressure difference between the inside and the outside of the bubble. However, when the aperture appears on the film, the gas inside the bubble is being released, and the pressure inside the bubble becomes equal to that of the atmosphere. As a result, the bubble film falls down by its own weight [*Debregeas et al.*, 1998; *da Silveira et al.*, 2000]. When the bubble film falls, the gas which has remained inside the bubble is being forced out through the aperture. This may cause the air flow. In our experiments, air flow is usually observed only when the liquid viscosity is large (≥7.8 Pa s) and the final aperture radius is smaller than the bubble radius.

[65] Figure 17a shows the propagation velocity of the pressure fluctuation as a function of the bubble volume. The velocity is calculated by using the distance between the liquid surface and the microphone, and the time between the appearance of the aperture and that in which the microphone detects a negative pressure peak. Figure 17a indicates that in most of the experiments, the propagation velocity is less than 3 m s^{-1}, which is much slower than the sound velocity, suggesting that the pressure fluctuation is air flow rather than sound. According to Bernoulli's equation, pressure fluctuation is related to the flow velocity. Assuming that the velocity of the fluctuation is $u_a \sim 1$ m s^{-1} and $\rho_a \sim 1.2$ kg m^{-3} and ignoring the compressibility of air, we can estimate the possible pressure fluctuation as $\Delta P \sim \rho_a u_a^2/2 \sim 0.6$ Pa. This is the same order of magnitude as the measured amplitude of the pressure fluctuation (Figures 17b and 17c).

[66] Figures 17b and 17c shows the amplitude of the measured pressure fluctuation, which is classified as air flow. In Figure 17, we recognize again that the amplitude of the pressure fluctuation measured by the lower microphone, which is denoted by circles, is much larger than that measured by the upper microphone, which is denoted by crosses, suggesting only the lower microphone records a large pressure fluctuation. Figures 17b and 17c shows that larger bubbles and thinner films can generate pressure fluctuation with a larger amplitude in most of the experiments. This may be because the larger bubbles supply larger flow volumes, and also because thinner films are more deformable and deflate faster.

[67] We thus conclude that when the aperture appears on the bubble film, gas inside the bubble flows out to the atmosphere. The gas inside the bubble loses the overpressure, and the bubble film falls due to its own weight. During film deflation, the tangential direction of the film which determines the direction of the surface tension changes, such that the aperture growth stops. The deflating film pushes the gas inside the bubble and causes the air flow, which is observed as a low-frequency pressure fluctuation.

6. Implications for Volcanic Airwaves

[68] In our experiments, we have shown that the aperture growth during bubble bursting generates an airwave and make a synthetic waveform for this airwave. We here generalize the synthetic waveform with two models of aperture growth. This is because measuring the aperture growth on a bubble film in a real magma is much more difficult than that in our experiments. Although there are few visual observations of bubbles bursting on a lava lake [e.g., *Dibble et al.*, 2008; *Gerst et al.*, 2008; *Jones et al.*, 2008], access to an active volcano is usually very limited. In addition, when bubble bursting occurs in a volcanic column, it is not possible to observe it.

[69] We use two models for the aperture growth as described in section 5.1. For a bubble in a real viscous magma, the results in Figure 11 suggest that the viscous model expressed in equation (8) is more appropriate. This model however is for a sustained bubble at the surface, and

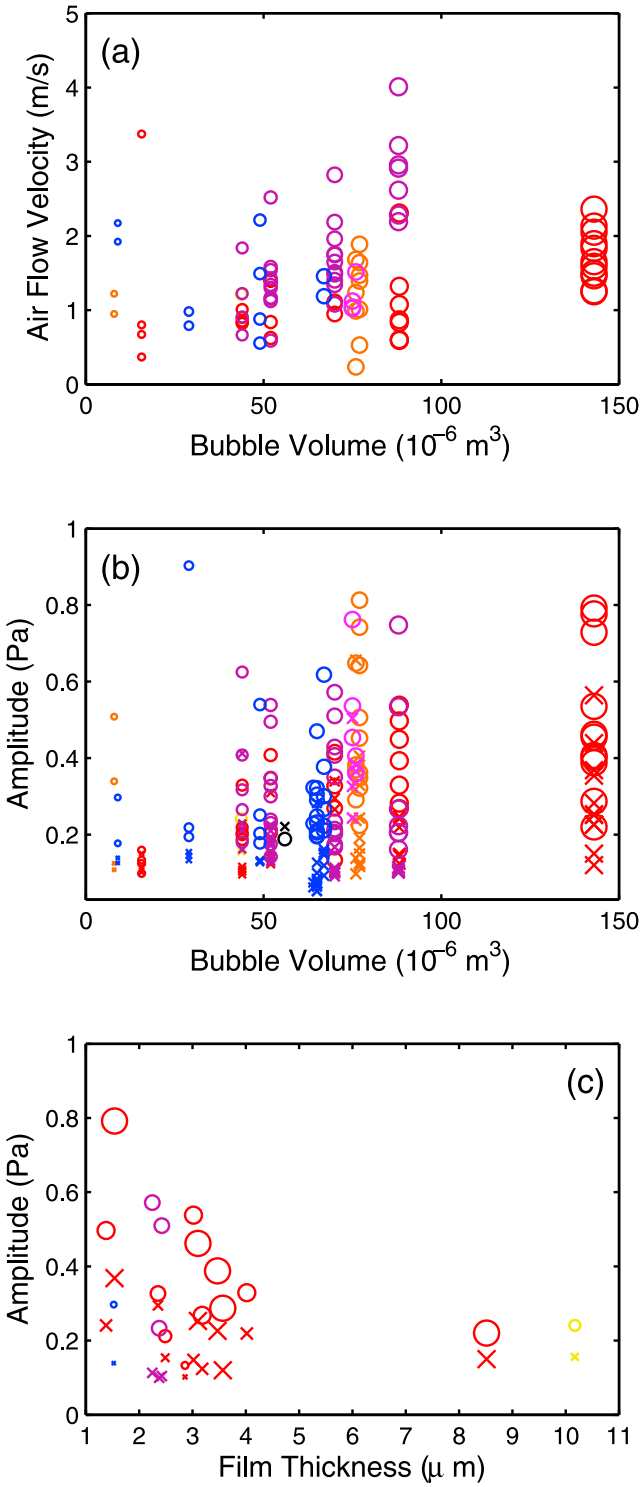

Figure 17. (a) Velocity of the air flow as a function of the bubble volume. (b) Measured amplitudes of the pressure fluctuations as a function of the bubble volume within 0.3 s after the aperture appears on the film. (c) Measured amplitudes of the pressure fluctuations as a function of bubble film thickness calculated in Figure 11. The symbols are the same as in Figure 9.

it is uncertain whether this is appropriate for an explosively expanding bubble. We thus first calculate the synthetic waveform using an inviscid model as a general case in which the aperture grows under a constant velocity [*Taylor*, 1959; *Culick*, 1960]. We then calculate using a viscous model which includes the acceleration of the aperture growth [*Debregeas et al.*, 1995, 1998].

6.1. A Synthetic Waveform Based on the Inviscid Model

[70] In order to calculate the synthetic waveform using equation (10), we should know the time-dependent pressure change in the bubble. When the aperture growth velocity is constant, by substituting $R = v_i t$ into equation (13) and integrating, we obtain

$$p(t) = p_0 \exp\left(\frac{-P_a \pi v_i^2 t^3}{3\rho_g c_g V}\right), \tag{14}$$

where p_0 is initial overpressure in the bubble. We here assume that the bubble is surrounded by a steam-based volcanic gas at 1100°C in which the gas density is ρ_g = 0.16 kg m^{-3} and the sound velocity is c_g = 870 m s^{-1}. In order to calculate the sound velocity, we use γ = 1.2 for high-temperature steam [*Kieffer and Sturtevant*, 1984]. An important feature of equation (14) is that when the aperture grows fast or when the bubble is small, the pressure inside the bubble drops quickly as shown in Figures 18a and 18b.

[71] From equations (10) and (14), we can calculate a synthetic waveform. Different from the synthetic waveform in our experiments, a in equation (10) should be the distance between the bubble and the observation point, and we use 1 km. In the experiments, the microphones are located in the acrylic pipe, so the surface area of airwaves cannot exceed the cross section of the pipe. However, the airwaves associated with volcanic eruptions are observed outside of the conduit and can spread hemispherically [e.g., *Garces et al.*, 1999] in the semi-infinite space (atmosphere). Here we use the retracted length of the film $v_i t$ as the aperture radius which also defines the size of the sound source growing until the bubble radius.

[72] Figure 18c shows the calculated synthetic waveform when the aperture grows under a constant velocity. An important result is that the frequency and the amplitude of the synthetic waveform differ when the aperture growth velocity and bubble size change, although we use uniform initial overpressure inside the bubble, 10^4 Pa. Faster aperture growths, which are drawn by red curves, generate higher-frequency and larger-amplitude pulses. On the other hand, smaller bubbles, which are drawn by thicker curves, generate a higher frequency but a smaller-amplitude airwave. Note that this synthetic waveform does not include any resonance on reflection and is applicable only for the first pulse of airwaves.

[73] Figure 18d shows the estimated frequency of the airwaves. We here assume that the half width of the pulse in Figure 18c is equivalent to the half cycle of the oscillation (Figure 16). When the aperture growth velocity is of the order of several meters per second, the frequency of the airwave becomes a few hertz, which agrees with the typical frequency of the airwaves associated with Strombolian

eruptions [e.g., *Vergniolle and Brandeis*, 1996; *Johnson et al.*, 2004].

[74] If the aperture growth velocity follows the inviscid model described in equation (7), we can estimate the bubble film thickness. The surface tension of basaltic magma is around 0.4 N m^{-1} [*Walker and Mullins*, 1981], and its density is around 2700 kg m^{-3} [*Spera*, 2000]. For a bubble whose aperture growth velocity is 1 m s^{-1}, its film thickness becomes 3×10^{-4} m. This thickness is very thin relative to the ejected particles, 20 mm at Stromboli and 150 mm at Etna [*Chouet et al.*, 1974; *McGetchin et al.*, 1974]. We infer that the aperture growth during the Strombolian eruption is not only driven by surface tension but also by bubble expansion, which may make the aperture growth faster than that estimated by the inviscid model.

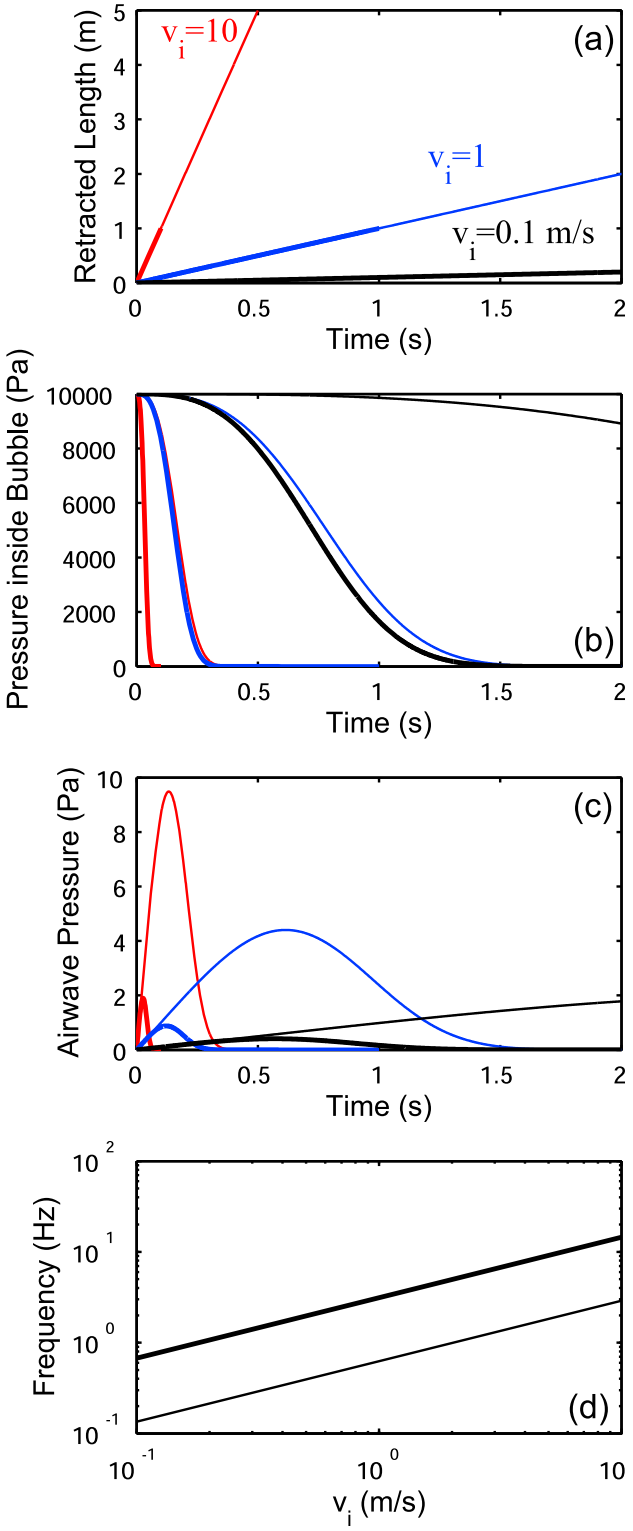

Figure 18. (a) Calculated retracted film length when the film edge moves at a constant velocity v_i. Black, blue, and red curves indicate v_i = 0.1,1, and 10 m s^{-1}, respectively. Thicker and thinner curves indicate a bubble radius of 1 and 5 m, respectively. (b) Calculated time evolution of overpressure inside the bubble for Figure 18a. (c) Calculated synthetic waveform observed 1 km away from the bubble. (d) Estimated frequency of airwaves as a function of the aperture growth velocities. Thick and thin lines indicate a bubble radius of 1 and 5 m, respectively.

6.2. A Synthetic Waveform Based on the Viscous Model

[75] Next, we calculate the synthetic waveform using the viscous model. By substituting equation (9) into equation (13) and integrating, we obtain

$$p = p_0 \exp\left[\frac{\pi P_a R_0^2}{\rho_g c_g V}\frac{\eta_m h}{2\sigma}\left\{1 - \exp\left(\frac{2t\sigma}{\eta_m h}\right)\right\}\right]. \quad (15)$$

From equations (9), (10), and (15), we obtain the analytical solution of the synthetic waveform.

[76] The aperture growth does not accelerate up to infinity. Once the growth velocity reaches the one calculated by the inviscid model, the acceleration should stop [*Debregeas et al.*, 1998]. On the other hand, the aperture growth stops at a certain radius, as shown in Figure 10 and reported by *Debregeas et al.* [1998] and *da Silveira et al.* [2000]. From Figure 13, we recognize that when the overpressure inside the bubble becomes close to zero, the aperture growth stops. We interpret this as that when the overpressure becomes zero, the bubble film begins deflation by its own weight. This changes the direction of the surface tension, and, as a consequence, the aperture growth loses its driving force and stops. We thus assume that the aperture growth stops when the overpressure drops to less than 1/100 of its initial value and use this to calculate the synthetic waveform. Note that this assumption does not affect the synthetic waveform.

[77] We calculate the aperture growth, including the above effects, as shown in Figure 19a. We here assume that magma viscosity to be 1, 10, and 100 Pa s which are value for low-viscosity basaltic magma [e.g., *Spera*, 2000]. For a bubble film thickness h, we use 0.02 m which is the typical size of ejected particles during a Strombolian eruption [e.g., *Chouet et al.*, 1974; *Houghton and Gonnermann*, 2008]. For the initial aperture radius, we assume a sufficiently small value of $R_0 = 10^{-4}$ m, which we find will not affect the synthetic waveform. The maximum aperture growth velocity for this condition is 0.12 m s^{-1}.

[78] Figure 19a shows that the aperture growth is slower for a more viscous magma. As a result, the overpressure inside the bubble drops slowly for a more viscous magma (Figure 19b). From equation (15), a thicker bubble film and

a smaller surface tension should behave in the same way as a more viscous magma. The pressure drop in a larger bubble is also slower. Figure 19c is the synthetic waveform calculated from Figures 19a and 19b. For the cases in which the bubble radius is 1 m (black thick line), we clearly recognize the effect of the aperture growth acceleration. When the magma is less viscous, the airwave which has larger amplitude and thinner pulse width arrives faster and vice versa for a more viscous magma. When the magma is more viscous (100 Pa s), the initial rise of the airwave becomes longer, and the waveform becomes asymmetric. A similar initial rise in airwaves associated with a real volcanic eruption has been reported [e.g., *Johnson et al.*, 2008]. This waveform represents the accelerating aperture growth (Figure 19a). For the cases in which the bubble radius is 5 m, the aperture growth continues even after its velocity reaches the upper limit v_i. As a result, the waveform for the cases with η = 1 and 10 Pa s becomes similar, but the airwave for the case with η = 1 Pa s arrives faster than that for the case with η = 10 Pa s.

[79] The characteristics of the airwave generated by the aperture growth are summarized in Figure 20. When the

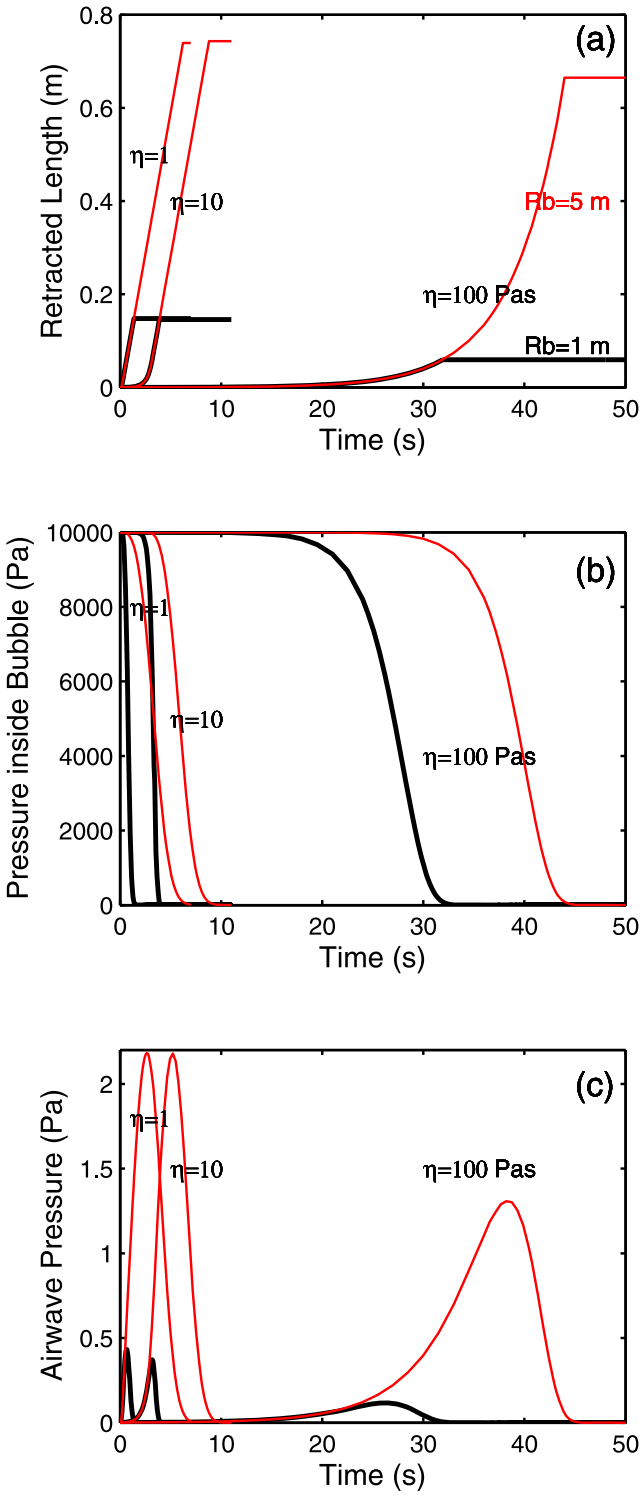

Figure 19. (a) Calculated retracted film length for the viscous model. First, the aperture growth follows equation (8). Once the growth velocity reaches the one calculated by the inviscid model v_i, the aperture grows at a constant velocity, v_i. When the overpressure inside the bubble drops, the aperture growth stops. We here assume that the magma viscosity is 1, 10, and 100 Pa s, the surface tension is 0.4 N m^{-1}, the density is 2700 kg m^{-3}, and the bubble film thickness is 0.02 m. The thick black curves and thin red curves indicate a bubble radius of 1 and 5 m, respectively. (b) Calculated pressure drop inside the bubble for Figure 19a. (c) Calculated synthetic waveform for Figures 19a and 19b observed 1 km away from the bubble.

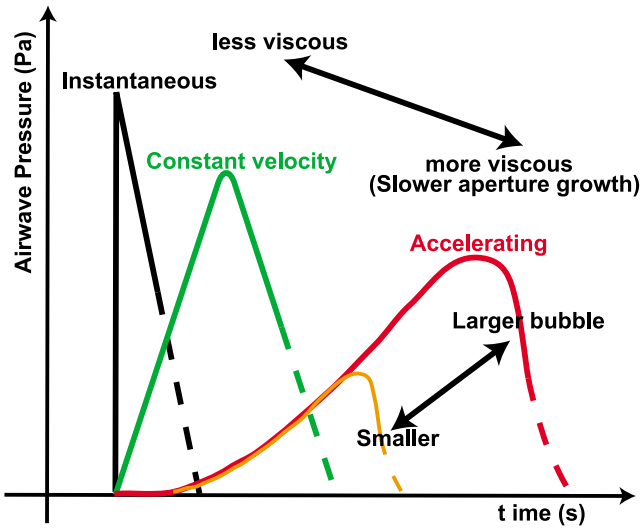

Figure 20. Schematic diagram summarizing how the waveform varies when the aperture growth and bubble size change under the same initial overpressure inside the bubble. When the bubble film surrounding a pressurized gas is removed instantaneously, the waveform becomes an N shape. The amplitude of the airwave represents the initial overpressure inside the bubble. When the aperture on the bubble film grows under a certain velocity, faster growth results in a higher frequency and larger amplitude. When the aperture growth accelerates, the waveform becomes asymmetric. A smaller bubble also makes the amplitude of the airwave smaller. These are applicable only for the first pulse, and the subsequent waveform depends on the resonant system.

aperture growth is slow, resulting airwaves have low frequency, which may explain the observed low frequency of the airwaves during Strombolian eruptions. One important application of this synthetic waveform is that we may be able to estimate the details of the bursting bubble from the airwaves. The initial rise of the waveform may represent the style in which the aperture grows which depends on the effective viscosity and the thickness of the bubble film as shown in equation (9). The pulse width and the amplitude depend on the aperture growth velocity and the bubble size. An important result is that the amplitude of the airwave does not necessarily represent the initial overpressure inside the bubble. When the bubble is small or the aperture grows slowly, the amplitude of the airwave becomes small even when the initial overpressure inside the bubbles are the same. In some cases, the amplitude may become smaller than the noise level. The volume of volcanic gas released from the bubble has been estimated using the waveform of the pressure waves [e.g., *Johnson et al.*, 2008]. Our experiments suggest that if the aperture growth is too slow and does not excite an observable airwave, the estimated amount of the released gas from the airwave may become an underestimate.

6.3. Differences Between Volcanic Airwaves and Models

[80] Both of the above two models do not quantitatively explain the observed frequency of the volcanic airwaves. As we discussed in section 6.1, when we use the inviscid model, the thickness of the bubble film needed to generate the typical frequency of the volcanic airwave becomes too thin. In the viscous model, the frequencies of the synthetic waveform in Figure 19 are also too low to explain an airwave generated by a bubble bursting in viscous magma. The frequencies of the airwaves observed during the explosion at Etna and Shishaldin are both around 1–2 Hz, although the magma viscosity for these volcanoes are different and are 10 and 500 Pa s, respectively [*Vergniolle and Caplan-Auerbach*, 2004; *Vergniolle and Ripepe*, 2008]. Our model however, predicts that a more viscous magma generates an airwave with a lower frequency.

[81] A possible cause of these discrepancies may be due to our model not including bubble expansion during the aperture growth. If a bubble expands during the period when the aperture exists on a bubble film, the growth rate of the aperture becomes larger than that driven by surface tension alone. Faster aperture growth results in a higher frequency. The effect of the bubble expansion may reconcile the discrepancy between the volcanic airwave and our model.

[82] In our current model, the bubble expansion is not included. Only surface tension is the driving force for aperture growth. Such kind of bubble bursting may not be able to erupt fragmented magma. Small infrasonic pulses are observed and the relation between the volcanic gas release has been discussed [*Ripepe and Gordeev*, 1999; *Ripepe et al.*, 2007]. This may be produced by bubble film rupture without radial bubble expansion. Our model may be better suited to explain such kind of volcanic gas release.

[83] Our model only explains the waveform of the initial positive pulse. Usually, airwaves associated with a volcanic eruption shows oscillation after the initial positive pulse. In our experiments, oscillation is generated by the resonance of the air column. This suggests that the continuous oscillation observed in an airwave during a volcanic eruption, is similarly generated by resonance. When the bubble bursts in the volcanic conduit, the conduit will act as a resonator. On the other hand, when a bubble bursts at the surface of a lava lake, no such permanent resonator is present. We note however, that after the bubble film disappears during bubble bursting, a cavity (concave depression) can remain at the surface of the viscous fluid. When the wavelength of the airwave caused by the aperture growth on the bubble film matches with the resonance frequency of the cavity, resonance can be excited [e.g., *Divoux et al.*, 2008]. If the cavity disappears immediately, there will be no such resonator, and the waveform would become that shown by solid curves in Figure 20.

6.4. Viscosity Range for Bubble Vibration

[84] In our experiments, vibration of bubbles is observed only when the liquid viscosity is low. This result is consistent with that of the previous study [*James et al.*, 2004]. This fact suggests that when the damping, which is related with the viscosity, is effective, the bubble does not vibrate. The viscous damping coefficient is expressed as [*Leighton*, 1994; *Vergniolle and Brandeis*, 1996]

$$\beta = \frac{6\eta_{\mathrm{liq}}}{\rho_{\mathrm{liq}} R_{\mathrm{b}}^2}, \tag{16}$$

which is the inverse of the timescale for the amplitude decay; that is, only oscillation with frequency of higher than β can be observed. This equation depends on both η_{liq} and R_{b}^{-2}, indicating that a larger bubble may be able to vibrate in a higher-viscosity liquid.

7. Conclusions

[85] We have performed experiments of bubble bursting at the surface of a viscous liquid contained in an acrylic pipe and measured the generated airwaves. Important experimental results are categorized into two groups by the liquid viscosity.

[86] When the liquid viscosity is less than 1 Pa s, the bubble film vibrates before the aperture appears on the bubble film. The aperture grows to the end of the film at a constant velocity. When the liquid viscosity is 10^{-3} Pa s, we observe high-frequency airwaves before an aperture appears on the bubble film. When the liquid viscosity is 0.17 Pa s, we observe a high-frequency airwaves which are generated after the aperture grows to the end of the film.

[87] On the other hand, when the liquid viscosity is larger than 1 Pa s, the bubble film does not vibrate prior to the appearance of an aperture. After an aperture appears, the aperture growth first accelerates, and then slows down, and finally the bubble deflates. The more viscous the liquid is, the slower the aperture grows. When the liquid viscosity is 1.9 Pa s, we observe air column resonance just after the aperture appears. When the liquid viscosity is 7.8–37 Pa s, we observe air column resonance just after the aperture appears and sometimes together with an airflow. When the liquid viscosity is in the range of 68–120 Pa s, we observe an airflow some time after the opening of the aperture.

[88] From these observations, we conclude that the major source of the airwave differs depending on the liquid vis-

cosity. When the liquid viscosity is low, the bubble film vibrates, and this becomes the major source of the airwave. When the liquid viscosity is high, the aperture growth on the bubble film generates the airwave. When the frequency of the airwave generated by the aperture growth matches the resonance frequency of the air column well, the air column resonance is excited and continues for a long time.

[89] We propose a model of an airwave generated by aperture growth. Synthetic waveforms explain the experimental observations well when the liquid viscosity is in the range of $1 < \eta_{liq} < 40$ Pa s. This model explains the experimentally observed facts, which show that a larger bubble or faster aperture growth generates larger-amplitude airwaves. We estimated volcanic airwaves with this model and found that when the aperture grows under a velocity of several m s^{-1}, the frequency of the airwave becomes a few hertz, which is observed during Strombolian eruptions. If the aperture growth accelerates, the initial rise of the airwave becomes gradual, and the waveform is asymmetric; these features are consistent with those also observed during Strombolian eruptions.

Notation

a pipe radius or distance between the bubble and the observation point (m).
c sound velocity (m s^{-1}).
f frequency (s^{-1}).
h bubble film thickness (m).
L length of the air column (m).
P_a atmospheric pressure (Pa).
P_b gas pressure inside the bubble (Pa).
p overpressure inside the bubble (Pa).
p_m overpressure measured by the microphone (Pa).
R_b bubble radius (m).
R aperture radius (m).
t time (s).
u gas flow velocity (m s^{-1}).
V volume of gas inside the bubble (m^3).
v aperture growth velocity (m s^{-1}).
γ ratio of specific heats.
ρ density (kg m^{-3}).
η viscosity (Pa s).
σ surface tension coefficient (N m^{-1}).

Subscripts

0 initial value
a air
i inviscid model.
v viscous model.
liq liquid.
g volcanic gas.
m magma.

[90] **Acknowledgments.** We thank S. Vergniolle, C. Matyska, and an anonymous reviewer for constructive comments; T. Watanabe and M. Ichihara for helpful advice; and N. Endo for providing the lamp used in the experiments. Part of this work was supported by Grants-in-Aid for Scientific Research, JSPS (grant 19740281).

References

Aster, R., S. Mah, P. Kyle, W. McIntosh, N. Dunbar, J. Johnson, M. Ruiz, and S. McNamara (2003), Very long period oscillations of Mount Erebus Volcano, *J. Geophys. Res.*, *108*(B11), 2522, doi:10.1029/2002JB002101.

Blackburn, E. A., L. Wilson, and R. S. J. Sparks (1976), Mechanisms and dynamics of Strombolian activity, *J. Geol. Soc.*, *132*, 429–440, doi:10.1144/gsjgs.132.4.0429.

Blackstock, D. T. (2000), *Fundamentals of physical acoustics*, 541 pp., Wiley-Interscience, New York.

Brenner, M. P., and D. Gueyffier (1999), On the bursting of viscous films, *Phys. Fluids*, *11*, 737–739, doi:10.1063/1.869942.

Buckingham, M. J., and M. A. Garces (1996), Canonical model of volcano acoustics, *J. Geophys. Res.*, *101*, 8129–8151, doi:10.1029/95JB01680.

Burton, M., P. Allard, F. Mure, and A. L. Spina (2007), Magmatic gas composition reveals the source depth of slug-driven Strombolian explosive activity, *Science*, *317*, 227–230, doi:10.1126/science.1141900.

Cannata, A., P. Montalto, E. Privitera, G. Russo, and S. Gresta (2009), Tracking eruptive phenomena by infrasound: May 13, 2008 eruption at Mt. Etna, *Geophys. Res. Lett.*, *36*, L05304, doi:10.1029/2008GL036738.

Caplan-Auerbach, J., and S. R. McNutt (2003), New insights into the 1999 eruption of Shishaldin volcano, Alaska, based on acoustic data, *Bull. Volcanol.*, *65*, 405–417, doi:10.1007/s00445-002-0267-5.

Chouet, B. (2003), Volcano seismology, *Pure Appl. Geophys.*, *160*, 739–788, doi:10.1007/PL00012556.

Chouet, B., N. Hamisevicz, and T. R. McGetchin (1974), Photoballistics of volcanic jet activity at Stromboli, Italy, *J. Geophys. Res.*, *79*, 4961–4976, doi:10.1029/JB079i032p04961.

Culick, F. E. C. (1960), Comments on a ruptured soap film, *J. Appl. Phys.*, *31*, 1128–1129, doi:10.1063/1.1735765.

da Silveira, R., S. Chaieb, and L. Mahadevan (2000), Rippling instability of a collapsing bubble, *Science*, *287*, 1468–1471, doi:10.1126/science.287.5457.1468.

Debregeas, G., P. Martin, and F. Brochard-Wyart (1995), Viscous bursting of suspended films, *Phys. Rev. Lett.*, *75*, 3886–3889, doi:10.1103/PhysRevLett.75.3886.

Debregeas, G., P. G. de Gennes, and F. Brochard-Wyart (1998), The life and death of "bare" viscous bubbles, *Science*, *279*, 1704–1707, doi:10.1126/science.279.5357.1704.

Deihl, D. T., and F. R. Carlson (1968), "N waves" from bursting balloons, *Am. J. Phys.*, *36*, 441–444, doi:10.1119/1.1974556.

Dibble, R. R., P. R. Kyle, and C. A. Rowe (2008), Video and seismic observations of Strombolian eruptions at Erebus volcano, Antarctica, *J. Volcanol. Geotherm. Res.*, *177*, 619–634, doi:10.1016/j.jvolgeores.2008.07.020.

Divoux, T., V. Vidal, F. Melo, and J. C. Geminard (2008), Acoustic emission associated with the bursting of a gas bubble at the free surface of a non-Newtonian fluid, *Phys. Rev. E*, *77*, 056310, doi:10.1103/PhysRevE.77.056310.

Edmonds, M. (2008), New geochemical insights into volcanic degassing, *Philos. Trans. R. Soc. A*, *366*, 4559–4579, doi:10.1098/rsta.2008.0185.

Garces, M. A., and S. R. McNutt (1997), Theory of the airborne sound field generated in a resonant magma conduit, *J. Volcanol. Geotherm. Res.*, *78*, 155–178, doi:10.1016/S0377-0273(97)00018-8.

Garces, M., M. Iguchi, K. Ishihara, M. Morrisey, Y. Sudo, and T. Tsutsui (1999), Infrasonic precursors to a vulcanian eruption at Sakurajima Volcano, Japan, *Geophys. Res. Lett.*, *26*, 2537–2540, doi:10.1029/1998GL005327.

Gerst, A., M. Hort, P. R. Kyle, and M. Voge (2008), 4D velocity of Strombolian eruptions and man-made explosions derived from multiple Doppler radar instruments, *J. Volcanol. Geotherm. Res.*, *177*, 648–660, doi:10.1016/j.jvolgeores.2008.05.022.

Hagerty, M. T., S. Y. Schwartz, M. A. Garces, and M. Protti (2000), Analysis of seismic and acoustic observations at Arenal volcano, Costa Rica, 1995–1997, *J. Volcanol. Geotherm. Res.*, *101*, 27–65, doi:10.1016/S0377-0273(00)00162-1.

Harris, A., and M. Ripepe (2007), Synergy of multiple geophysical approaches to unravel explosive eruption conduit and source dynamics—A case study from Stromboli, *Chem. Erde*, *67*, 1–35, doi:10.1016/j.chemer.2007.01.003.

Hellweg, M. (2000), Physical models for the source of Lascar's harmonic tremor, *J. Volcanol. Geotherm. Res.*, *101*, 183–198, doi:10.1016/S0377-0273(00)00163-3.

Houghton, B. F., and H. M. Gonnermann (2008), Basaltic explosive volcanism: Constrains from deposits and models, *Chem. Erde*, *68*, 117–140, doi:10.1016/j.chemer.2008.04.002.

Ichihara, M., M. Ripepe, A. Goto, H. Oshima, H. Aoyama, M. Iguchi, K. Tanaka, and H. Taniguchi (2009), Airwaves generated by an underwater explosion: Implications for volcanic infrasound, *J. Geophys. Res.*, *114*, B03210, doi:10.1029/2008JB005792.

James, M. R., S. J. Lane, B. Chouet, and J. S. Gilbert (2004), Pressure changes associated with the ascent and bursting of gas slugs in liquid-filled vertical and inclined conduits, *J. Volcanol. Geotherm. Res.*, *129*, 61–82, doi:10.1016/S0377-0273(03)00232-4.

James, M. R., S. J. Lane, and B. A. Chouet (2006), Gas slug ascent through changes in conduit diameter: Laboratory insights into a volcano-seismic source process in low-viscosity magmas, *J. Geophys. Res.*, *111*, B05201, doi:10.1029/2005JB003718.

Jaupart, C., and S. Vergniolle (1988), Laboratory models of Hawaiian and Strombolian eruptions, *Nature*, *331*, 58–60, doi:10.1038/331058a0.

Johnson, J. B., R. C. Aster, and P. R. Kyle (2004), Volcanic eruptions observed with infrasound, *Geophys. Res. Lett.*, *31*, L14604, doi:10.1029/2004GL020020.

Johnson, J., R. Aster, K. R. Jones, P. Kyle, and B. McIntosh (2008), Acoustic source characterization of impulsive Strombolian eruptions from the Mount Erebus lava lake, *J. Volcanol. Geotherm. Res.*, *177*, 673–686, doi:10.1016/j.jvolgeores.2008.06.028.

Jones, K. R., J. B. Johnson, R. Aster, P. R. Kyle, and W. C. McIntosh (2008), Infrasonic tracking of large bubble bursts and ash venting at Erebus volcano, Antarctica, *J. Volcanol. Geotherm. Res.*, *177*, 661–672, doi:10.1016/j.jvolgeores.2008.02.001.

Kieffer, S. W., and B. Sturtevant (1984), Laboratory studies of volcanic jets, *J. Geophys. Res.*, *89*, 8253–8268, doi:10.1029/JB089iB10p08253.

Kulkarny, V. A. (1978), Impulsive discharge noise: Balloon burst problem and engine exhaust pulses, *J. Acoust. Soc. Am.*, *64*, 298–301, doi:10.1121/1.381975.

Lees, J. M., E. I. Gordeev, and M. Ripepe (2004), Explosions and periodic tremor at Karymsky volcano, Kamchatka, Russia, *Geophys. J. Int.*, *158*, 1151–1167, doi:10.1111/j.1365-246X.2004.02239.x.

Leighton, T. G. (1994), *The Acoustic Bubble*, 613 pp., Academic, San Diego, Calif.

Lindfors, K. R. (1924), Surface tension of sugar factory products, *Ind. Eng. Chem.*, *16*, 813–816, doi:10.1021/ie50176a018.

McGetchin, T. R., M. Settle, and B. A. Chouet (1974), Cinder cone growth modeled after northeast crater, Mount Etna, Sicily, *J. Geophys. Res.*, *79*, 3257–3272, doi:10.1029/JB079i023p03257.

Morrissey, M. M., and B. A. Chouet (1997), Burst conditions of explosive volcanic eruptions recorded on microbarographs, *Science*, *275*, 1290–1293, doi:10.1126/science.275.5304.1290.

Namiki, A., and M. Manga (2005), Response of a bubble bearing viscoelastic fluid to rapid decompression: Implications for explosive volcanic eruptions, *Earth Planet. Sci. Lett.*, *236*, 269–284, doi:10.1016/j.epsl.2005.02.045.

Namiki, A., and M. Manga (2008), Transition between fragmentation and permeable outgassing of low viscosity magmas, *J. Volcanol. Geotherm. Res.*, *169*, 48–60, doi:10.1016/j.jvolgeores.2007.07.020.

Neuberg, J., R. Luckett, M. Ripepe, and T. Braun (1994), Highlights from a seismic broadband array on Stromboli volcano, *Geophys. Res. Lett.*, *21*, 749–752, doi:10.1029/94GL00377.

Parfitt, E. A. (2004), A discussion of the mechanisms of explosive basaltic eruptions, *J. Volcanol. Geotherm. Res.*, *134*, 77–107, doi:10.1016/j.jvolgeores.2004.01.002.

Ripepe, M., and E. Gordeev (1999), Gas bubble dynamics model for shallow volcanic tremor at Stromboli, *J. Geophys. Res.*, *104*, 10,639–10,654, doi:10.1029/98JB02734.

Ripepe, M., P. Poggi, T. Braun, and E. Gordeev (1996), Infrasonic waves and volcanic tremor at Stromboli, *Geophys. Res. Lett.*, *23*, 181–184, doi:10.1029/95GL03662.

Ripepe, M., S. Ciliberto, and M. D. Schiava (2001), Time constraints for modeling source dynamics of volcanic explosions at Stromboli, *J. Geophys. Res.*, *106*, 8713–8727, doi:10.1029/2000JB900374.

Ripepe, M., E. Marchetti, and G. Ulivieri (2007), Infrasonic monitoring at Stromboli volcano during the 2003 effusive eruption: Insights on the explosive and degassing process of an open conduit system, *J. Geophys. Res.*, *112*, B09207, doi:10.1029/2006JB004613.

Rowe, C. A., R. C. Aster, P. R. Kyle, R. R. Dibble, and J. W. Schlue (2000), Seismic and acoustic observations at Mount Erebus volcano, Ross Island, Antarctica, 1994–1998, *J. Volcanol. Geotherm. Res.*, *101*, 105–128, doi:10.1016/S0377-0273(00)00170-0.

Seyfried, R., and A. Freundt (2000), Experiments on conduit flow and eruption behavior of basaltic volcanic eruptions, *J. Geophys. Res.*, *105*, 23,727–23,740, doi:10.1029/2000JB900096.

Spera, F. J. (2000), Physical properties of magma, in *Encyclopedia of Volcanoes*, edited by H. Sigurdsson, pp. 171–190, Academic, San Diego, Calif.

Spiel, D. E. (1992), Acoustical measurements of air bubbles bursting at a water surface: Bursting bubbles as Helmholtz resonators, *J. Geophys. Res.*, *97*, 11,443–11,452, doi:10.1029/92JC00982.

Taylor, G. (1959), The dynamics of thin sheets of fluid III, disintegration of fluid sheets, *Proc. R. Soc. London, Ser. A*, *253*, 313–321, doi:10.1098/rspa.1959.0196.

Vergniolle, S., and G. Brandeis (1994), Origin of the sound generated by Strombolian explosions, *Geophys. Res. Lett.*, *21*, 1959–1962, doi:10.1029/94GL01286.

Vergniolle, S., and G. Brandeis (1996), Strombolian explosions: 1. A large bubble breaking at the surface of a lava column as a source of sound, *J. Geophys. Res.*, *101*, 20,433–20,447, doi:10.1029/96JB01178.

Vergniolle, S., and J. Caplan-Auerbach (2004), Acoustic measurements of the 1999 basaltic eruption of Shishaldin volcano, Alaska: 2. Precursor to the subplinian phase, *J. Volcanol. Geotherm. Res.*, *137*, 135–151.

Vergniolle, S., and M. Ripepe (2008), From Strombolian explosions to fire fountains at Etna Volcano (Italy): What do we learn from acoustic measurements?, in *Fluid Motions in Volcanic Conduits: A Source of Seismic and Acoustic Signals*, edited by S. J. Lane and J. S. Gilbert, *Geol. Soc. Spec. Publ.*, 307, 103–124, doi:10.1144/SP307.7.

Vergniolle, S., G. Brandeis, and J.-C. Mareschal (1996), Strombolian explosions: 2. Eruption dynamics determined from acoustic measurements, *J. Geophys. Res.*, *101*, 20,449–20,466, doi:10.1029/96JB01925.

Vidal, V., J. C. Geminard, T. Divoux, and F. Melo (2006), Acoustic signal associated with the bursting of a soap film which initially closes an overpressurized cavity, *Eur. Phys. J. B*, *54*, 321–339, doi:10.1140/epjb/e2006-00450-0.

Walker, D., and J. O. Mullins (1981), Surface tension of natural silicate melts from 1200°–1500°C and implications for melt structure, *Contrib. Mineral. Petrol.*, *76*, 455–462, doi:10.1007/BF00371487.

Wilson, L. (1980), Relationships between pressure, volatile content and ejecta velocity in three types of volcanic explosion, *J. Volcanol. Geotherm. Res.*, *8*, 297–313, doi:10.1016/0377-0273(80)90110-9.

Yokoo, A., and H. Taniguchi (2004), Application of video image processing to detect volcanic pressure waves: A case study on archived images of Aso Volcano, Japan, *Geophys. Res. Lett.*, *31*, L23604, doi:10.1029/2004GL021183.

Yoshikawa, S., and H. Fujita (2002), *Fundamental Acoustics (in Japanese)*, 269 pp., Kodansha, Tokyo.

T. Kobayashi and I. Sumita, Division of Earth and Environmental Sciences, Graduate School of Natural Science and Technology, Kanazawa University, Kakuma, Kanazawa, Ishikawa 920-1192, Japan. (sumita@hakusan.s.kanazawa-u.ac.jp)

A. Namiki, Department of Earth and Planetary Science, University of Tokyo, 7-3-1 Hongo, Bunkyo-ku, Tokyo 113-0033, Japan. (namiki@eps.s.u-tokyo.ac.jp)